

Nanoscale Advances

Accepted Manuscript

This article can be cited before page numbers have been issued, to do this please use: M. M. Aboelnga, R. G. Elbayaa, E. Elbayoumy, M. Garavelli and M. Eltahawy, *Nanoscale Adv.*, 2026, DOI: 10.1039/D6NA00232C.



This is an Accepted Manuscript, which has been through the Royal Society of Chemistry peer review process and has been accepted for publication.

Accepted Manuscripts are published online shortly after acceptance, before technical editing, formatting and proof reading. Using this free service, authors can make their results available to the community, in citable form, before we publish the edited article. We will replace this Accepted Manuscript with the edited and formatted Advance Article as soon as it is available.

You can find more information about Accepted Manuscripts in the [Information for Authors](#).

Please note that technical editing may introduce minor changes to the text and/or graphics, which may alter content. The journal's standard [Terms & Conditions](#) and the [Ethical guidelines](#) still apply. In no event shall the Royal Society of Chemistry be held responsible for any errors or omissions in this Accepted Manuscript or any consequences arising from the use of any information it contains.

Metal-decorated Graphdiyne Nanocarriers for Favipiravir Delivery: A DFT Investigation

Mohamed M. Aboelnga^{1+*}, Rana G. Elbayaa¹⁺, Elsayed Elbayoumy¹, Marco Garavelli², Mohsen Eltahawy³

¹Chemistry Department, Faculty of Science, Damietta University, New Damietta 34517, Egypt.

²Dipartimento di Chimica Industriale "Toso Montanari" Via Piero Gobetti 85, University of Bologna, Italy

³Chemistry Department, Faculty of Science, Damanhur University, 22511, Damanhur Egypt.

Corresponding Author: mohamed-aboelnga@du.edu.eg

+Equal Contribution to this work

Abstract:

Favipiravir (FAV) is a broad-spectrum antiviral whose therapeutic efficacy is limited by poor bioavailability, motivating the development of nanoscale delivery platforms. Herein, density functional theory (DFT) calculations are employed to systematically investigate the adsorption behavior of FAV on pristine and transition-metal-decorated graphdiyne (GDY) nanosheets. Ni, Cu, and Ti modifiers are introduced to tune interfacial interactions at the atomic scale. Calculations at the B3LYP/6-31G(d) level, in both gas and implicit solvent environments, reveal that pristine GDY enables moderate, reversible physisorption (-0.26 eV; 2.45 Å), suitable for controlled release. In contrast, metal decoration significantly strengthens adsorption, with FAV(N/O)-GDY-Ni, -Cu, and -Ti exhibiting binding energies of -4.41 , -3.96 , and -6.03 -5.79 eV, respectively, alongside reduced interaction distances. Electronic structure analyses (FMO, DOS, NBO, and RDG-NCI) confirm enhanced charge transfer and interaction localization upon metal incorporation, supported by thermodynamic favorability. These findings highlight metal-decorated GDY as a tunable nanoplatform for improving drug loading and stability, offering computational framework for guiding future experimental work.

Keywords: Favipiravir drug, Graphdiyne nanosheet, Drug delivery, Decoration, Nanocarriers, DFT study.



1. Introduction

Favipiravir (FAV) was originally developed and approved for the treatment of influenza virus infections (1). Favipiravir is an antiviral drug that selectively inhibits RNA-dependent RNA polymerase (RdRp) of RNA viruses (2). It was discovered while screening chemical library for ~~anti-viral~~ antiviral effects on the influenza virus by Toyama Chemical Co., Ltd (2). Favipiravir is effective toward various types and subtypes of influenza viruses (3). It also exhibits antiviral properties against other RNA viruses, including filoviruses, arenaviruses, and bunyaviruses (4). Because of its distinct antiviral properties, favipiravir has the potential to be a promising treatment for untreatable RNA viral infections (4). It has shown efficacy against many RNA viruses, including Ebola virus, Lassa virus, norovirus and enterovirus (5–8).

Additionally, favipiravir is approved for emergency use to treat COVID-19 disease (9–14). The SARS-CoV-2 virus is responsible for COVID-19 disease, which infects human instantaneously (15). This evolution from influenza treatment to a key therapeutic candidate for emerging RNA virus outbreaks exemplifies favipiravir's unique broad-spectrum antiviral profile and therapeutic promise. But like many drugs, it has some limitations, such as low bioavailability and side effects, which reduce its therapeutic effectiveness. Some reported side effects include diarrhea, elevated transaminase levels, hyperuricemia, nausea, thrombocytopenia and neutropenia (16, 17). To overcome these challenges advanced drug delivery systems employing nanomaterials have been developed. Drug delivery systems have attracted significant attention due to their ability to deliver precise amounts of drugs at specific target sites in the human body (18), minimizing the risk of side effects so drug delivery nanocarriers are essential for enhancing drug bioavailability and therapeutic effectiveness in treating specific viruses and diseases.

Various nanoparticles including gold nanoparticles, liposomes, silicone nanoparticles, carbon nanotubes, natural and synthetic polymers, as well as magnetic nanoparticles, have recently been employed for drug delivery applications (19, 20). Carbon materials such as fullerenes, carbon nanotubes, and graphene, in addition to their modified forms, have gained important attention recently as useful tools in medicine, especially as carriers that work for drug delivery (21, 22). Since their nanoscale dimensions permit them to penetrate biological membranes more easily, they improve drug transport along with help drugs stay in the body longer. Since carbon nanomaterials do have distinctive structural and physicochemical features, they stand out as superb platforms that allow for the development of advanced drug delivery systems (23, 24). These candidates are strong to make therapeutic delivery approaches that are more effective and efficient (25, 26). In addition, their performance is strongly influenced by the nature of intermolecular



interactions governing drug adsorption and release. Intermolecular interactions play a fundamental role in determining the efficiency of drug-nanocarrier systems. The adsorption, stability, and release behavior of drug molecules are mainly governed by non-covalent interactions such as hydrogen bonding, π - π stacking, van de Waals forces, and electrostatic interactions. These interactions are particularly important in carbon-based nanocarriers, where π -conjugated surfaces enable strong yet reversible binding with aromatic or heterocyclic drug molecules. A balanced interaction strength is essential to ensure efficient drug loading while allowing controlled release at the target site. Therefore, understanding these intermolecular forces at the molecular level is crucial for designing effective nanocarriers with optimized therapeutic performance (27).

Graphdiyne (GDY) is a novel two-dimensional carbon-based nanomaterial with unique structural and physicochemical properties, including high surface area, tunable electrical conductivity, uniform pores, strong π -conjugation, high thermal stability, thermal conductivity, excellent biocompatibility, and low toxicity, which make it suitable for biomedical applications (28–30). Compared with other carbon nanomaterials such as graphene, carbon nanotubes, and fullerenes, graphdiyne (GDY) possesses uniformly distributed intrinsic pores and a mixed sp/sp^2 hybridized carbon network, which provide additional active adsorption sites and facilitate stronger interactions with drug molecules (31). These unique structural characteristics make GDY a particularly promising nanocarrier for enhanced drug loading and controlled drug release. Graphdiyne (GDY) has been widely investigated in biosensing, cancer therapy, drug delivery, wound healing, radiation protection, and tissue engineering, among these applications, its role in drug delivery is significant as graphdiyne (GDY) can load therapeutic molecules through π - π stacking and electrostatic interactions and release them in a controlled and targeted way (28–30, 32–35). These qualities enable graphdiyne (GDY) to improve the solubility, stability, and controlled release of drug at the target site, and enhancing therapeutic efficacy while decreasing toxicity. Studies show graphdiyne (GDY) nanosheets can effectively deliver drugs such as cisplatin drug (36), Flutamide drug (37), Imuran, Pentasa and Hyoscyamine drugs (38), Temozolomide drug (39), Hydroxyurea and 5-Fluorouracil drugs (40). Additional functional improvements of graphdiyne (GDY) as a drug carrier can be achieved by decorating its nanosheet with transition metals. Metal decoration provides new active sites and modifies the electronic structure of the carbon nanosheets, which in turn enhances drug loading efficiency, targeting specificity, and therapeutic efficacy. The modified electronic properties enhance the



adsorption energies and molecular interactions between graphdiyne and drug molecule, resulting in a more stable drug-nanocarrier complex and enabling controlled drug release(41–48).

Despite extensive DFT studies on Favipiravir adsorption over carbon nanomaterials such as graphene (49), carbon nanotubes (50), and fullerenes (51), the interaction of favipiravir with graphdiyne (GDY), particularly in its metal decorated forms, remains largely unexplored. In this study, a computational method density functional theory (DFT) was employed to investigate the adsorption of favipiravir on pristine and metal-decorated graphdiyne (GDY) as a carrier for the antiviral drug favipiravir. For decoration we use transition metals nickel (Ni), copper (Cu) and titanium (Ti). The choice of the specified transition metals for decoration on graphdiyne (GDY) due to their affinity to form stable complexes with organic compounds (52), as well as their ability to modulate their distinct electronic characteristics and interaction behavior with carbon-based systems. Ni exhibits strong d- π hybridization leading to stable binding and significant electronic coupling. Cu provides moderate interaction strength with relatively electronic conductivity, while Ti offers high chemical reactivity and significant charge transfer, allowing a systematic evaluation of metal-dependent effect on adsorption behavior (53). In addition, these transition metals have been widely employed in previous theoretical studies on carbon-based nanomaterials, where they were shown to significantly influence adsorption properties and electronic structure modulation(54–57). Recent studies have revealed that density functional theory (DFT) provides valuable insights into molecular structure and their interactions (58). Density functional theory (DFT) has been widely used to explore drug-nanocarrier interactions, particularly through the calculation of adsorption energies and analysis of molecular interactions (59–63). These parameters offer important details about the strength and stability of drug binding, which support the design of more effective drug delivery systems. Researchers can refine the molecular structure of nanocarriers to enhance their targeting capabilities and therapeutic efficacy in various biomedical applications. This can lead to improved treatment outcomes and more effective delivery of drugs (64, 65). To enhance the understanding of adsorption processes, additional analyses were performed. Molecular orbital analysis, including (HOMO-LUMO) and corresponding energy gaps, was employed to evaluate the electronic reactivity and charge transfer capability upon adsorption. Natural bond orbital (NBO) analysis was performed to determine donor-acceptor interactions and intramolecular charge delocalization, providing a detailed description of the stabilization arising from orbital interactions. Furthermore, density of states (DOS) analysis was used to investigate the changes in the electronic structure of the system. Infrared (IR) spectroscopy simulations



were conducted to identify vibrational characteristics associated with adsorption. Additionally reduced density gradient and non-covalent interaction (RDG-NCI) analyses were performed to visualize and distinguish weak intermolecular forces, such as van der Waals forces and hydrogen bonding. Thermodynamic parameters were evaluated to assess the stability of adsorption process. Moreover, work function was performed to evaluate the influence of adsorption on the surface electronic properties. The goal of our research is to explore the properties of geometric parameters, adsorption energies, and various electrical and geometric characteristics using DFT.

2. Computational methods

Density functional theory (DFT) used to investigate the adsorption behavior of favipiravir drug on pristine and metal-decorated graphdiyne surfaces in gas and water phases. For optimization of geometry and analysis of electronic properties and energy computations along with the associated computations the B3LYP exchange–correlation functional was used together with the 6-31G(d) basis set (66), as implemented in the Gaussian 09 software package (67). This level of theory was selected due to its well-established balance between accuracy and computational efficiency and have been successfully used for the treatment of similar chemical systems. Visualization and analysis of optimized geometries were performed using Gauss View 6.0. However, unrestricted calculations were employed for the Cu complexes, as the presence of unpaired electrons. DFT was selected for this study because it provides an excellent balance between computational efficiency and accuracy in describing the electronic structure of complex systems. DFT offers reliable insights into adsorption energies, electronic distributions, and intermolecular interactions at a reasonable computational cost. This makes it particularly suitable for investigating drug adsorption on nanomaterial surfaces(68–80). The electronic properties were performed to evaluate the stability of the FAV–GDY complexes, including highest molecular orbital (HOMO) and lowest unoccupied molecular orbital (LUMO). Density of states (DOS), infrared (IR) spectra were analyzed using Gauss Sum. Reduced density gradient–noncovalent interaction (RDG–NCI) analysis to explore noncovalent interactions. Frequency calculations were performed to explore intermolecular interactions and to obtain the thermodynamic parameters associated with the adsorption process, including enthalpy change (ΔH), Gibbs free energy change (ΔG) and entropy (ΔS). Frequency calculations have been done on all chemical systems at the same level of theory for the optimization. All optimized structures were confirmed to correspond to true global minimum on the potential energy surface, as verified by vibrational frequency calculations showing no imaginary frequencies, indicating that the structures were



actually minima. Through the analysis of adsorption energies and molecular descriptors, these calculations offered valuable insight into adsorption mechanisms.

The adsorption energy (E_{ad}) of the favipiravir molecule on pristine graphdiyne surface is calculated, for the selected configurations, through the following equation:

$$E_{ads} = E_{GDY/FAV} - (E_{GDY} + E_{FAV}) \quad (1)$$

Here, E_{GDY} is the total energy of graphdiyne, E_{FAV} is the total energy of favipiravir, and $E_{FAV/GDY}$ is the total energy of favipiravir adsorbed on graphdiyne surface, where negative values indicate favorable adsorption.

To improve the accuracy of the calculated interaction energies, basis set superposition error (BSSE) was corrected using the counterpoise method, as defined by the following equation:

$$E_{ads} = E_{GDY/FAV} - (E_{GDY} + E_{FAV}) + E_{BSSE} \quad (2)$$

The energy gap between HOMO and LUMO (E_g) and Fermi level energy are defined as follows:

$$E_{gap} = E_{LUMO} - E_{HOMO} \quad (3)$$

$$E_F = \frac{E_{LUMO} + E_{HOMO}}{2} \quad (4)$$

Where, E_{LUMO} and E_{HOMO} are energy of highest occupied molecular orbital (HOMO) and lowest unoccupied molecular orbital (LUMO).

3. Result and discussion

3.1. Different optimized adsorption geometries of Favipiravir on GDY surface

The interaction of favipiravir with the GDY nanosheet was explored through the optimization of different orientations. This approach enabled the identification of the most stable adsorption geometry and provided clearer insight into how the drug interacts with the GDY surface. Five different orientations of the drug molecule were investigated and optimized, as shown in **Fig. 1**. In Tilted-OH orientation (**Fig. 1a**), the hydroxyl group directed closer to the GDY surface, with interaction distances of 2.53 Å between hydrogen and carbon atom and 3.35 Å between oxygen atom and carbon. This arrangement allows simultaneous π - π stacking and dipole-dipole interactions. In Vertical-OH (**Fig. 1b**) hydroxyl remains the main contact site with the GDY surface, larger interaction distances observed, 2.84 Å between hydrogen and carbon



atom and 3.40 Å between oxygen atom and carbon, reflecting a weaker adsorption efficiency. In NH₂/F-oriented (**Fig. 1c**), the drug molecule oriented perpendicularly to the GDY surface, the NH₂ and F groups are directed toward the surface, enabling additional polar interactions with the GDY surface. The interaction distances were 2.90 Å between the hydrogen of the NH₂ group and the GDY surface, and 3.26 Å between the fluorine atom and the GDY surface. In Carbonyl-side (**Fig. 1e**), the FAV shows adsorption along the edge of the GDY surface, where contact is established mainly through side interactions, this orientation supported mainly by weak van der Waals forces, with interaction distances of 2.34 Å between the carbonyl group and the hydrogen of the GDY nanosheet, and 3.49 Å between the nitrogen atom of the pyrazine ring and the carbon of the GDY nanosheet. The contact is less stable and less uniform compared to the other orientations. In Hydroxyl-side (**Fig. 1d**) the hydroxyl group is directed toward the edge of the GDY nanosheet creating hydrogen bond and dipole-dipole interactions, in addition to van der Waals interactions, with interaction distances of 2.45 Å between the oxygen atom and the hydrogen of the GDY nanosheet, and 2.51 Å between the hydrogen atom and the carbon of the GDY nanosheet. The hydroxyl-OH configuration was found to be the most stable orientation in Vacuum with adsorption energy -0.26 eV, and shorter interaction distances compared to the other adsorption modes.

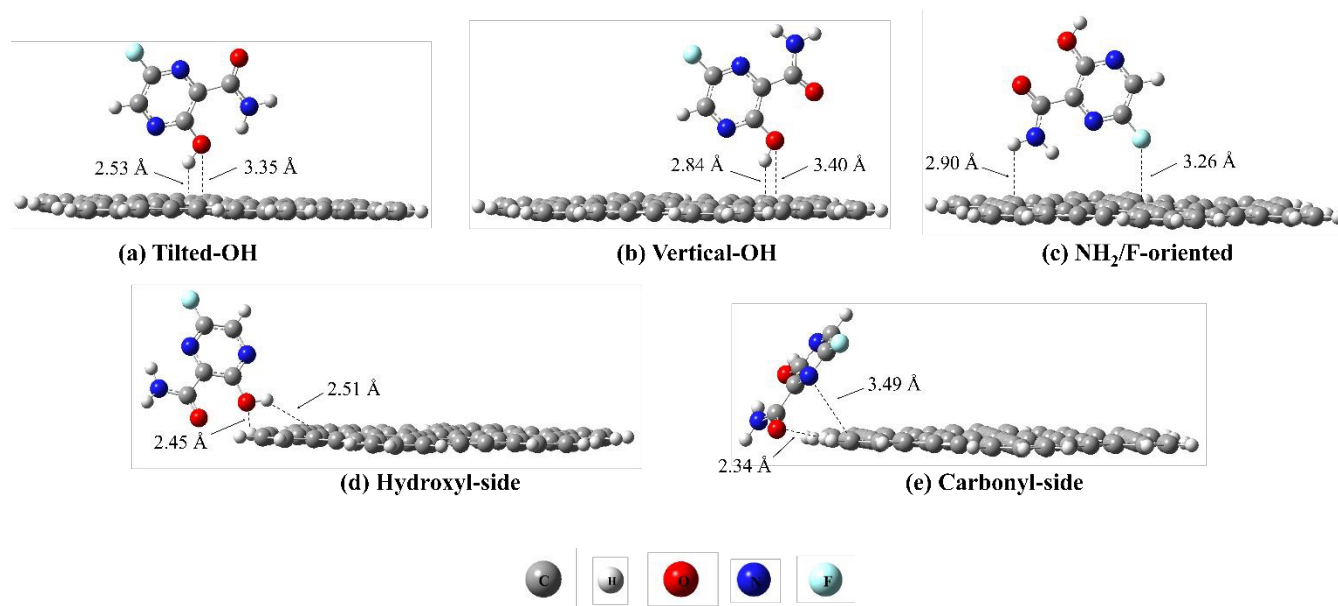


Figure 1. Optimized geometries of FAV drug on GDY nanosheet in five orientations, highlighting variations in molecular alignment and interaction sites responsible for adsorption behavior (in gas phase).



To further enhance this interaction and explore possible improvements in carrier efficiency, metal decoration was subsequently introduced to the GDY framework. The decorated models were optimized using the same computational protocol, allowing a direct and reliable comparison with the pristine systems. This stepwise strategy not only clarifies how surface functionalization modifies the adsorption landscape but also demonstrates the extent to which decoration can strengthen the drug carrier interaction.

3.2. Optimized geometries of FAV on decorated GDY

To explore the impact of the decorated systems on the binding of our drug, the interaction between the drug and each decorated model has been carefully modeled. Two different orientations for each metal-decorated GDY have been obtained and thus a total of six models were identified. The optimized configurations of favipiravir on Ni, Cu, and Ti-decorated GDY are presented in **Fig. 2**, where two adsorption orientations were obtained for each metal. These geometries reveal how metal anchoring sites restructure the interaction landscape and significantly modify the binding characteristics of the drug. The interaction distances and corresponding adsorption energies highlight how the drug adopts different geometries to optimize binding. Across all systems, the first orientation consistently exhibits a more favorable adsorption energy, indicating a stronger and more stable interaction compared to the second orientation.

For Ni-decorated GDY, the adsorption of favipiravir is stabilized through direct coordination between the metal center and heteroatoms of the drug molecule. In the first orientation the Ni atom interacts with the nitrogen and oxygen atoms of favipiravir, forming Ni-O and Ni-N coordination bonds with interaction distances of 1.89 Å and 1.92 Å, respectively, these short interaction distances indicate strong metal-ligand coupling and result in a highly stable adsorption configuration. In the second orientation the Ni atom forms Ni-O and Ni-N coordination bonds with distances of 1.91 Å and 2.25 Å, respectively, remain within the range of strong surface coordination, the slightly elongated second distance corresponds to a less negative adsorption energy value.

In case of Cu-decorated GDY surface, the adsorption mechanism is similarly governed by coordination between Cu atom and heteroatoms of favipiravir. In the first orientation, the drug molecule establishes Cu-O and Cu-N interactions with distances of 1.98 Å and 2.01 Å, respectively. In the second orientation, the coordination framework remains intact, characterized by Cu-O and Cu-N coordination with interaction distances of 1.90 Å and 2.78 Å, respectively.



For the Ti-decorated GDY, the adsorption of favipiravir is dominated by coordination interactions involving oxygen and nitrogen atoms. The first orientation exhibits Ti-O and Ti-N interactions with distances of 1.95 Å and 2.26 Å, respectively. In second orientation the interaction is characterized by Ti-O and Ti-N coordination with distances of 2.16 Å and 2.01 Å respectively. The adsorption behavior of favipiravir on the decorated GDY surfaces reveals a clear enhancement in interaction strength when metal decoration is introduced. All decorated systems exhibit markedly stronger adsorption energies compared to pristine GDY sheet, indicating that surface modification creates highly active binding centers capable of forming stronger drug-carrier interactions. The decorated structures show strong interactions, confirming the effectiveness of the modification strategy.

Among the evaluated systems, the FAV(N/O)-GDYNi, FAV(N/O)-GDYCu and FAV(N/O)-GDYTi complexes **Fig. 2 (a-c)**, demonstrate the highest binding affinity toward favipiravir, indicating a substantial stabilization of favipiravir on the decorated nanosheet. These findings demonstrate that the metal decoration alters the electronic structure and reactivity of GDY, creating coordination sites capable of interacting with the oxygen and nitrogen atoms of favipiravir. The resulting interactions are considerably stronger than those observed on the pristine GDY surface, which supports the idea that decoration not only enhances binding affinity but also offers tunability depending on the selected metal.

Overall, the decorated GDY systems exhibit the essential characteristics of an efficient nanocarrier. The significant increase in adsorption energy relative to the pristine sheet underscores the promising potential of decorated-GDY as a highly effective nanocarrier for favipiravir, offering improved stability and stronger binding essential for efficient drug delivery applications.



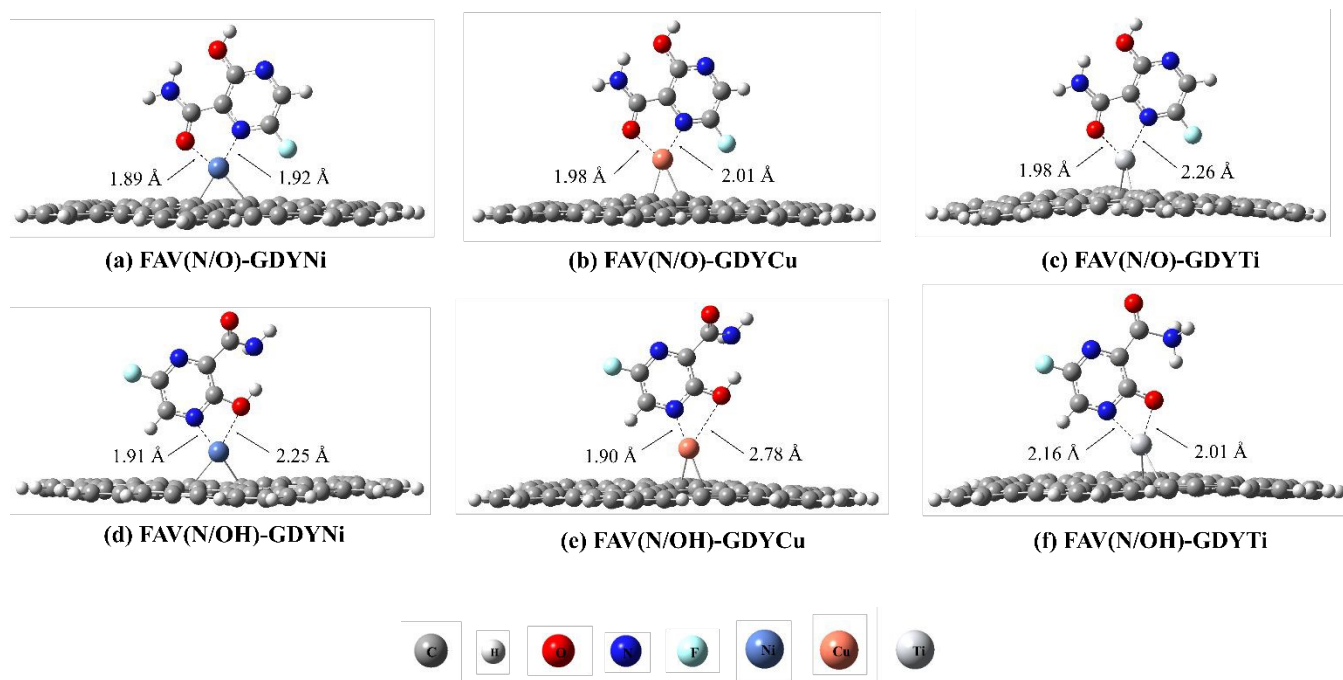


Figure 2. Optimized geometries for different adsorption orientations of FAV on decorated-GDY surfaces: Ni-GDY, Cu-GDY and Ti-GDY, with their interaction distances in gas phase.

3.3. Frontier molecular orbital analysis

The frontier molecular orbitals (FMOs), namely the highest occupied molecular orbital (HOMO) and the lowest unoccupied molecular orbital (LUMO), offer a detailed understanding of the electronic distribution and interaction mechanism between favipiravir and the GDY nanosheet. As shown in **Fig. 3 and 4**, the HOMO electron density is mainly localized on the favipiravir molecule, particularly around the oxygen and nitrogen sites, while the LUMO density is predominantly distributed over the GDY surface. The observed spatial separation of HOMO and LUMO orbitals reflect a pronounced donor-acceptor character within the FAV-GDY system, in which the favipiravir acts as the electron donor and GDY serves as the electron acceptor. For Cu complexes, both α - and β -spin configuration were analyzed, however, only the α -spin HOMO and LUMO are presented, as it demonstrates more pronounced variation in the electronic structure, it exhibits larger band gap values compared to β -spin configuration (see **Table 5**). The electron transfer tendency is further supported by the alignment of molecular orbitals, the localization of the LUMO on GDY nanosheet facilitates charge transfer from the drug molecule toward the nanosheet upon adsorption. This implies that the adsorption process involves charge transfer through non-covalent interactions, enhancing the stability of the complex. The delocalization of the LUMO orbitals across the



π -system of GDY indicates its strong capacity to accept electrons, while the confinement of the HOMO on favipiravir highlights its donor character arising from the heteroatoms and functional groups such as NH_2 , OH and $\text{C}=\text{O}$. These findings provide a deep understanding of the electronic features governing favipiravir adsorption on GDY and support its potential as adsorption material.

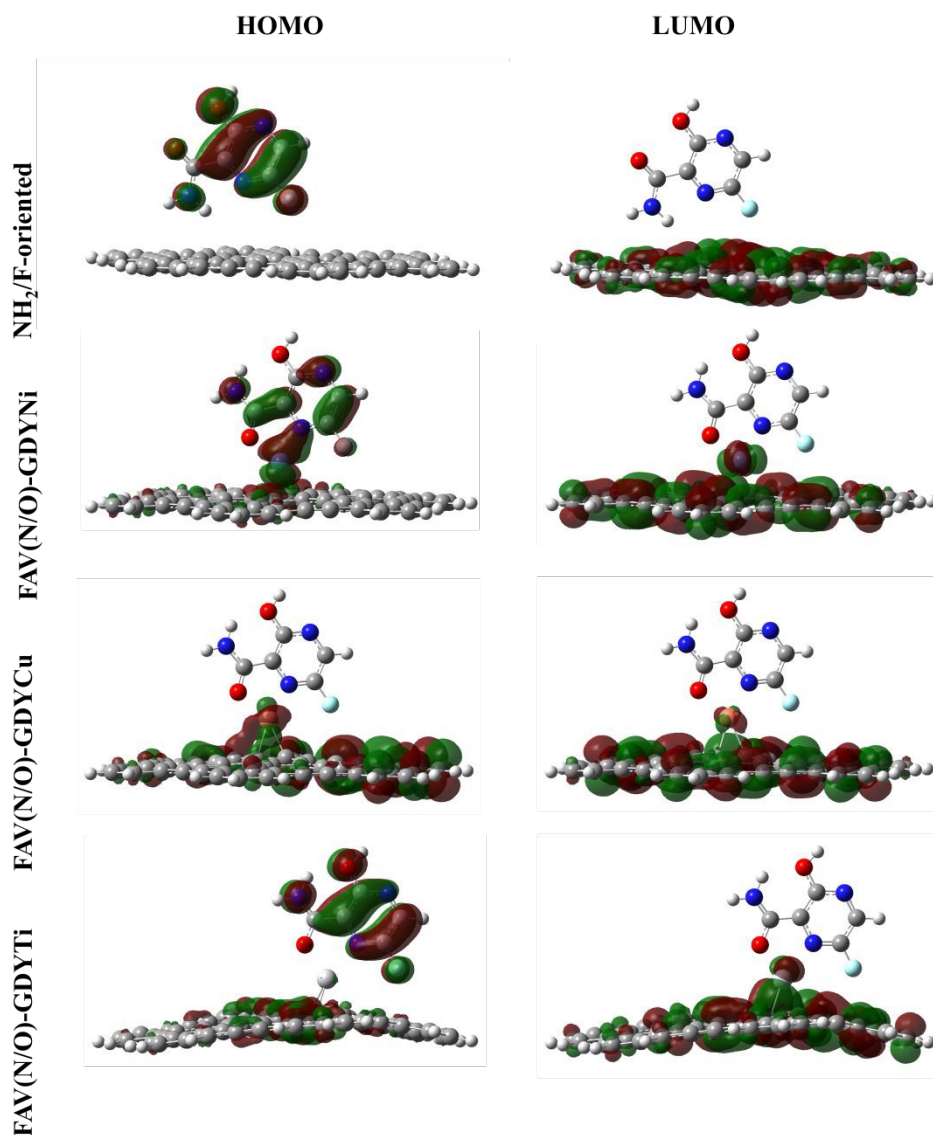


Figure 3. The distributions of molecular orbitals HOMO and LUMO of NH_2/F -oriented, FAV(N/O)-GDYNi, FAV(N/O)-GDYCu and FAV(N/O)-GDYTi complexes.



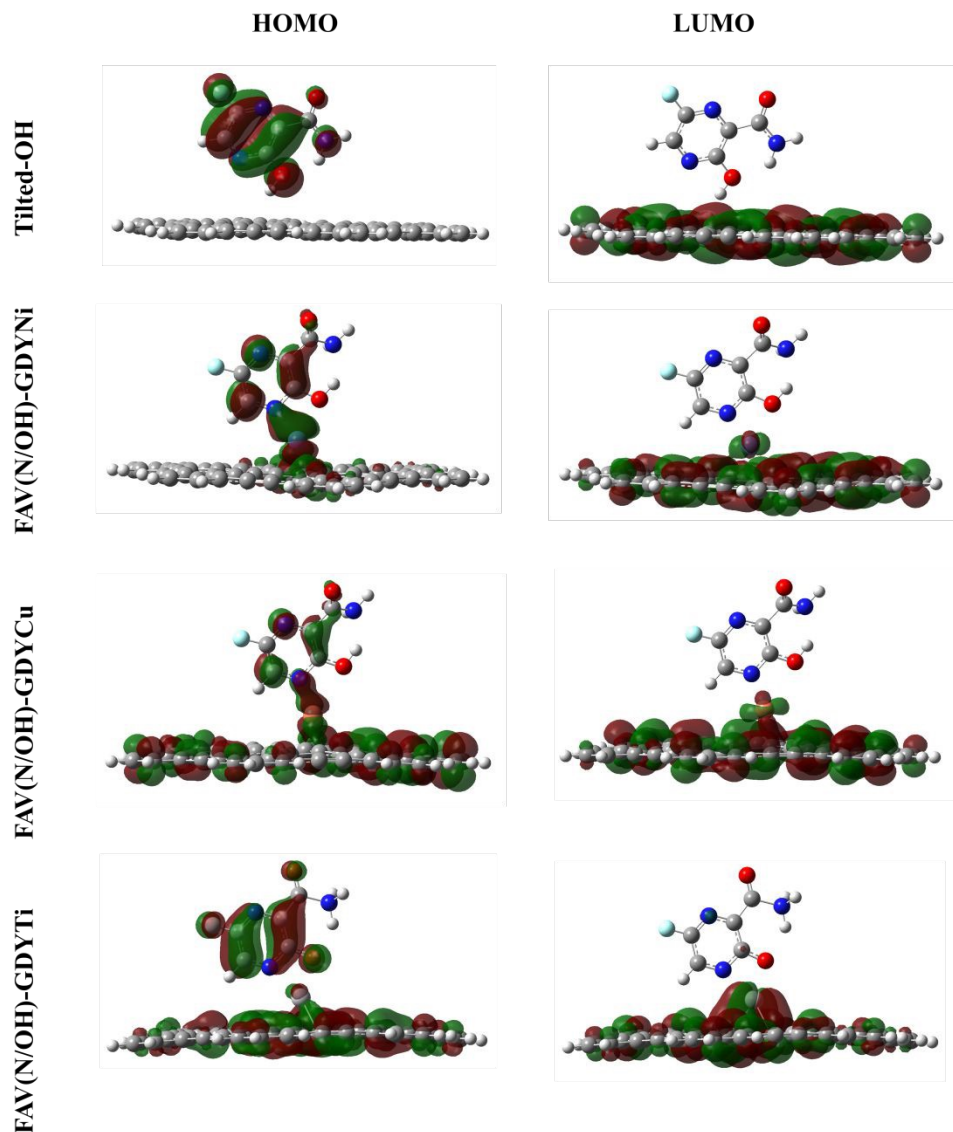


Figure 4. The distributions of molecular orbitals HOMO and LUMO of the Tilted-OH, FAV(N/OH)-GDYNi, FAV(N/OH)-GDYCu and FAV(N/OH)-GDYTi complexes.

3.4. Electronic and vibrational analysis (DOS and IR)

The combined analysis of the Density of states (DOS) and infrared (IR) spectra provides comprehensive insight into both the electronic structure and vibrational behavior of molecular system. DOS analysis reveals detailed information about electronic distribution and orbital interactions (81–85). The DOS spectra illustrate how the molecule orbitals of the drug interact with those of the nanosheet, revealing the nature of the electronic coupling in the system. The DOS profile shows a continuous distribution of states



around the Fermi level, suggesting an effective overlap between the orbitals of the favipiravir and those of the nanosheet. The infrared (IR) spectra were also analyzed to identify vibrational changes associated with adsorption and to confirm stability of the optimized geometries. **Fig. 5, 6** presented the simulated spectra, where distinct vibrational modes corresponding to characteristic functional groups of favipiravir, such as C=O, N–H, and C–F stretching vibrations. When studied together, DOS and IR analyses reveal both the electronic changes and structural stability resulting from molecular adsorption, which are critical in evaluating the suitability of nanomaterials for drug delivery.

The electronic properties were further analyzed using energy gaps (E_g), and Fermi level (E_F), which provide detailed insight into the interaction between favipiravir (FAV) and GDY-based nanostructures, as illustrated in Table 5. For the pristine GDY–FAV configurations, the calculated energy gaps fall within a narrow range of 2.498–2.611 eV, while the Fermi level varies slightly between –4.128 and –3.844 eV. These minor variations indicate weak interaction and limited charge transfer between FAV and the pristine GDY surface, with negligible perturbation in the electronic structure.

In contrast, the metal-decorated GDY–FAV complexes exhibit a pronounced modification in electronic properties. For FAV(N/O)-GDY_{Ni}, the energy gap decreases significantly to 0.813 eV with E_F at –9.422 eV. The FAV(N/O)-GDY_{Cu} systems show moderate E_g values of 1.531 eV and 1.019 eV, with corresponding E_F values of –8.832 eV and –9.059 eV, depending on the adsorption configuration. Notably, the FAV(N/O)-GDY_{Ti} complex exhibits the lowest energy gap (0.328 eV) with a deeply shifted Fermi level (–14.248 eV), indicating strong electronic interaction and superior charge transfer capability. A similar trend is observed for FAV(N/OH)-GDY_{Ni}, which shows E_g of 0.724 eV and E_F of –9.406 eV. For FAV(N/OH)-GDY_{Cu}, the energy gap varies significantly depending on the configuration, ranging from 2.159 to 0.596 eV, with E_F values between –8.837 and –9.572 eV, indicating configuration-dependent interaction strength. Meanwhile, FAV(N/OH)-GDY_{Ti} maintains a low E_g of 0.344 eV with E_F at –14.091 eV, confirming the stability of its enhanced electronic behavior.

Overall, the pristine GDY–FAV systems exhibit weak interaction characterized by minor changes in E_g and E_F , whereas metal-decorated systems especially Ti-based complexes show a substantial reduction in energy gap and significant shifts in Fermi level. This indicates strong orbital hybridization and efficient charge transfer upon adsorption, which is expected to induce notable changes in DOS and enhance the suitability of these systems.



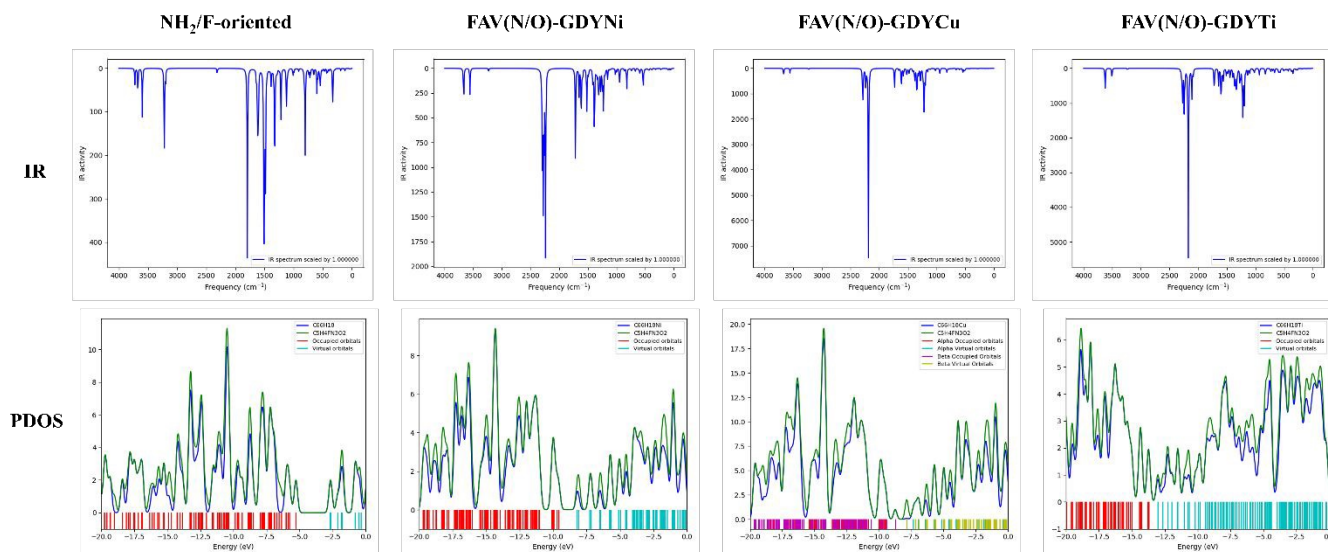


Figure 5. IR spectra and PDOS for NH₂/F-oriented, FAV(N/O)-GDYNi, FAV(N/O)-GDYCu and FAV(N/O)-GDYTi complexes.

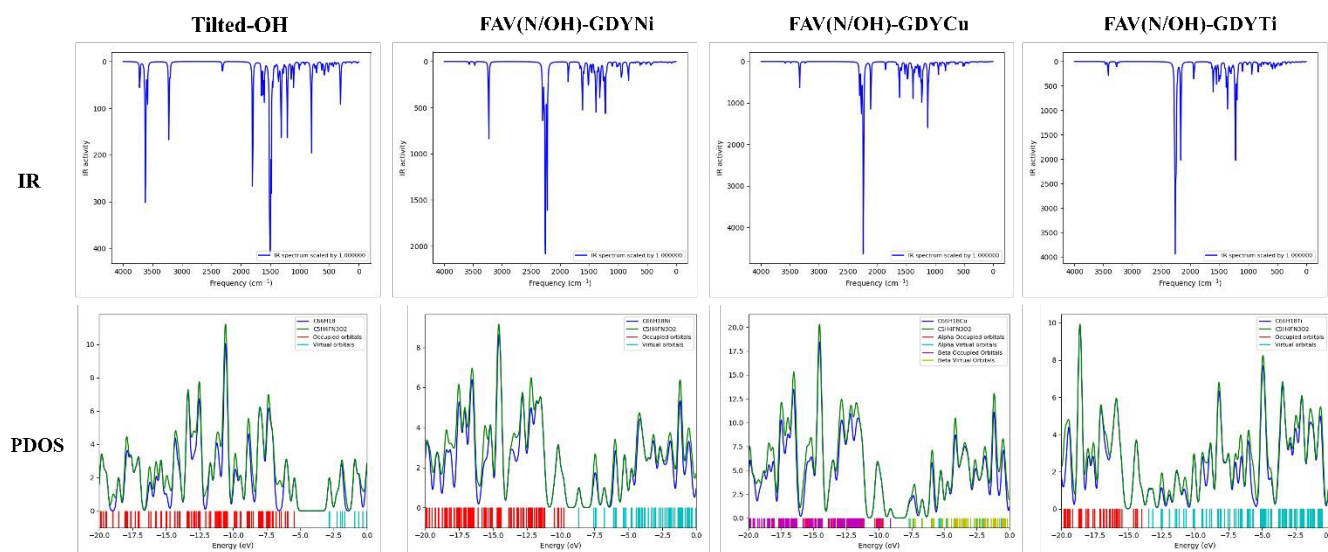


Figure 6. IR spectra and PDOS for tilted-OH, FAV(N/OH)-GDYNi, FAV(N/OH)-GDYCu and FAV(N/OH)-GDYTi complexes.

3.5. Non-covalent interactions (NCI)



The non-covalent interaction (NCI) analysis combined with the reduced density gradient (RDG) plots was employed to elucidate the nature and strength of interactions between the favipiravir and the GDY surface. These analyses provide a clear visualization of the weak intermolecular forces responsible for stabilizing the drug-GDY complexes, such as van der Waals interaction, hydrogen bonding, and steric repulsions (86–91). It is important to note that NCI analysis is inherently limited to non-covalent interactions and does not account for covalent bonding or charge-transfer effects. Accordingly, for pristine GDY, where adsorption is dominated by weak interactions, NCI provides an appropriate description. In contrast, for metal-decorated GDY systems, additional covalent contributions arising from metal–drug interactions are expected but are not captured by NCI analysis. The NCI isosurface of the optimized configurations of FAV on pristine and decorated-GDY clearly demonstrates regions of intermolecular interaction. As shown in **Fig.7,8**, the visualization of NCI reveals predominant green region at the drug-surface interface, signifying that van der Waals forces are the main contributors to the stabilization of the drug on GDY nanosheet. This observation reflects the dominant non-covalent component of interaction and should not be interpreted as evidence of purely physisorptive binding, particularly in the decorated systems. The RDG scatter plots allow the identification of different types of non-covalent interactions through the sign (λ_2) ρ descriptors and color mapping. The blue regions suggest the presence of attractive hydrogen bonding between the oxygen or nitrogen atoms of FAV and the carbon atoms on GDY, while red areas correspond to repulsive steric effect arising from short interatomic distances. The distribution and intensity of these colored isosurface reveal that all configurations are stabilized mainly through non-covalent interactions, typically associated with hydrogen bond, while red areas correspond to repulsion steric effect. The RDG is a function that mainly depends on the electron density (ρ) and the second derivative of the electron ($\Delta^2\rho$), which is calculated using this equation:

$$\text{RDG}(r) = \frac{1}{2(3\pi^2)^{1/3}} \frac{|\nabla\rho(r)|}{\rho(r)^{4/3}} \quad (5)$$

where ρ represents the electron density and $\Delta\rho$ is its gradient at a given point. Low values of the reduced density gradient in regions of low electron density indicate the presence of non-covalent interactions. To differentiate between attractive, van der Waals, and repulsive interactions, the sign of the second eigenvalue of the electron density Hessian (λ_2) multiplied by ρ was considered. In the resulting RDG-NCI plots and isosurfaces, blue regions corresponded to strong attractive interactions such as hydrogen bonding, green regions indicated weak van der Waals interactions, and red regions represented steric repulsion. The analysis revealed that the complexes were stabilized predominantly by van der Waals



forces, with hydrogen bonding contributing to additional stabilization, while steric repulsions were minimal. This visualization not only confirms the presence and type of non-covalent interactions but also provides insights into the spatial distribution of these interactions, which is critical for understanding the structural and energetic behavior of the complexes. However, when considered alongside the large binding energies, NBO stabilization energies, and work function shifts, it is evident that stronger interactions particularly in metal-decorated systems also involve partial covalent character and charge transfer. Therefore, adsorption on pristine GDY can be described as physisorption, whereas adsorption on metal-decorated GDY follows a mixed mechanism involving both non-covalent and chemisorption contributions.

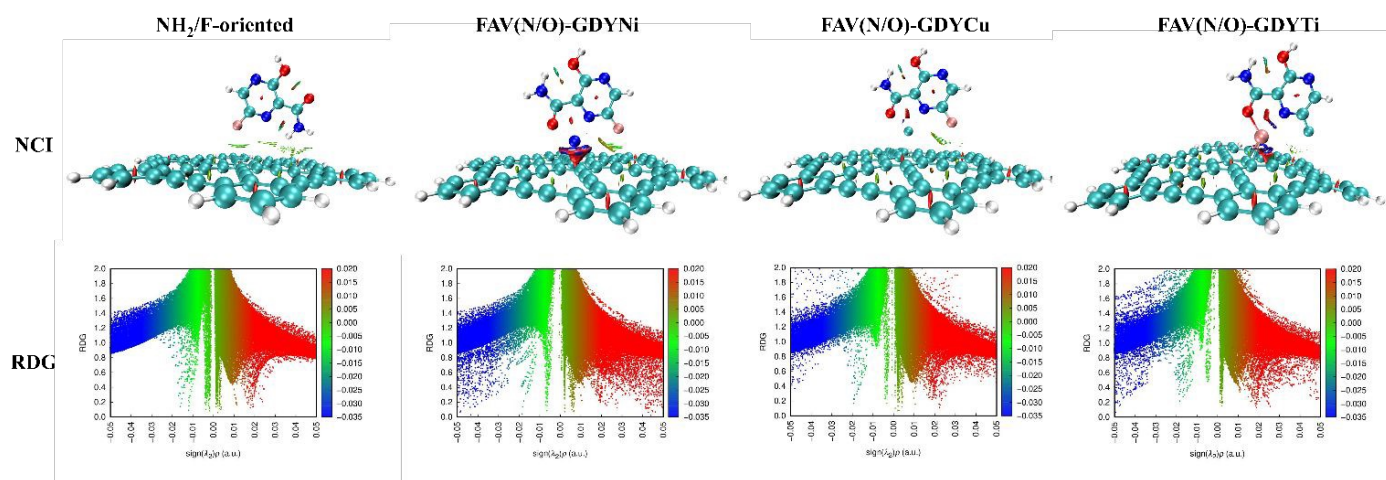


Figure 7. Non-Covalent Interaction (NCI), Reduced Density Gradients (RDG) for NH_2/F -oriented, FAV(N/O)-GDYNi, FAV(N/O)-GDYCu and FAV(N/O)-GDYTi complexes.



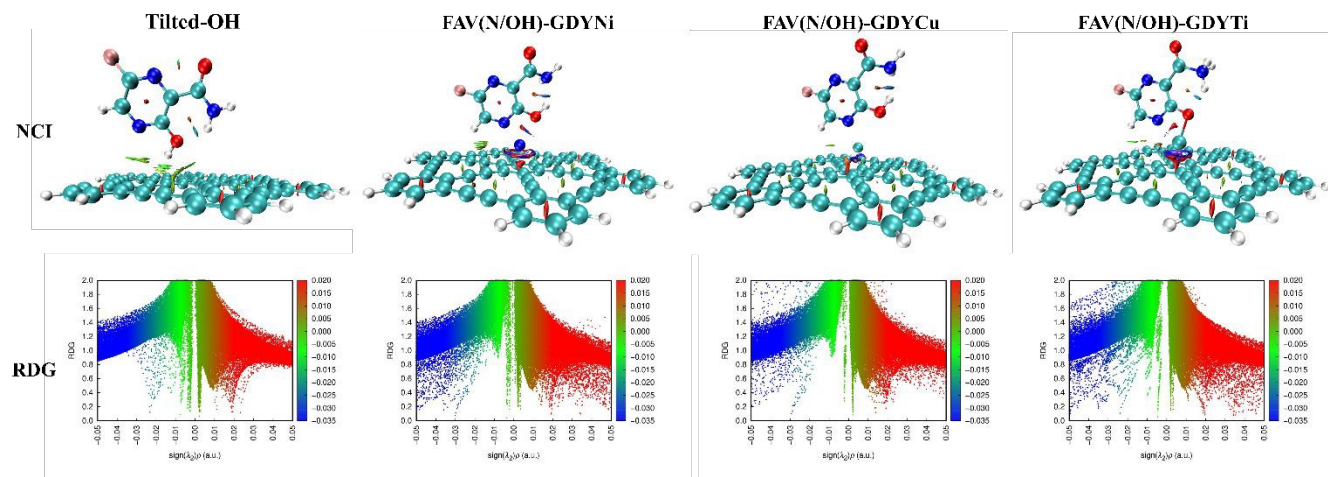


Figure 8. Non-Covalent Interaction (NCI), Reduced Density Gradients (RDG) for tilted-OH, FAV(N/OH)-GDYNi, FAV(N/OH)-GDYCu and FAV(N/OH)-GDYTi complexes.

3.6. Thermodynamic parameters

Thermodynamic analysis provides valuable insights into the energetic and spontaneous nature of the adsorption process between favipiravir and the graphdiyne surfaces. The calculated thermodynamic parameters, including Gibbs free energy (ΔG), enthalpy change (ΔH) and entropy change (ΔS), in both the gas and water phases are summarized in **Table 1**.

For pristine GDY surface, all examined orientations exhibit positive ΔG values, indicating that adsorption does not occur spontaneously whereas the ΔH values are slightly exothermic. This difference arises because the binding energy reflects only the electronic stabilization upon adsorption, whereas the Gibbs free energy also includes thermal and entropic contributions. For pristine GDY, these thermal effects outweigh the electronic stabilization, resulting in a positive ΔG value demonstrating a nonspontaneous process.

When the GDY surface is decorated with metal atoms, a notable enhancement in the thermodynamic behavior is observed. All decorated systems exhibit negative ΔG values, confirming the spontaneous nature of adsorption after modification. The significantly large negative ΔH values highlight the stronger and more stabilized interactions. The observed negative ΔS values for all complexes indicate a decrease in randomness upon adsorption.



The enthalpy change (ΔH) and Gibbs free energy change (ΔG) were calculated at $T = 298.15$ K and $P = 1$ atm as follows:

$$\Delta G = G_{GDY/FAV} - (G_{GDY} + G_{FAV}) \quad (6)$$

$$\Delta H = H_{GDY/FAV} - (H_{GDY} + H_{FAV}) \quad (7)$$

$$\Delta S = \frac{\Delta H - \Delta G}{298.15} \quad (8)$$

Table 1. The calculated thermodynamic parameters, Gibbs free energy (ΔG), enthalpy (ΔH) and entropy (ΔS) of all studied complexes in (KJ/mol), FAV drug with pristine and metal decorated GDY nanosheets, in gas phase as well as in water, respectively.

Structure	Gas			Water		
	ΔG	ΔS	ΔH	ΔG	ΔS	ΔH
Tilted-OH	17.45	-0.11	-16.82	30.37	-0.12	-4.31
Vertical-OH	18.03	-0.10	-10.86	31.05	-0.11	-2.57
NH₂/F-oriented	26.47	-0.12	-8.62	44.54	-0.17	-4.93
Hydroxyl-side	16.90	-0.12	-19.47	31.35	-0.12	-4.79
Carbonyl-side	25.74	-0.13	-13.45	31.51	-0.12	-5.35
FAV(N/O)-GDYNi	-366.72	-0.15	-411.15	-224.23	-0.14	-267.20
FAV(N/O)-GDYCu	-327.23	-0.14	-369.67	-220.36	-0.17	-272.33
FAV(N/O)-GDYTi	-519.41	-0.17	-570.17	-189.69	-0.18	-244.75
FAV(N/OH)-GDYNi	-214.39	-0.15	-259.53	-89.51	-0.18	-142.08
FAV(N/OH)-GDYCu	-218.12	-0.13	-256.77	-130.57	-0.17	-181.54
FAV(N/OH)-GDYTi	-489.12	-0.19	-544.30	-38.47	-0.19	-95.42

3.7. Solvent effect

To clarify the adsorption behavior in the presence of a polar environment. The geometries of the FAV drug with GDY and metal decorated GDY complexes were reoptimized in the water medium by utilizing the Integral Equation Formalism Polarizable Continuum Model (IEFPCM) method, applying the hydride B3LYP functional along with the 6-31G(d) basis set. The structural response of all systems was examined



upon introducing water as the solvent. As shown in **Fig. 9,10**, geometry optimizations showed that both pristine and metal-decorated GDY retain the same structural features with interatomic distances remaining close to those observed in the gas phase, confirming that the implicit solvent does not induce any noticeable geometric changes to the optimized models. An exception is observed for the FAV(N/OH)-GDYTi complex in gas phase **Fig. 2: (f)**, where an intramolecular hydrogen shift occurs, leading to the formation of a new bond between the hydrogen atom and nitrogen atom within the same molecule. Moreover, the effect of water as the solvent was evaluated through the calculated binding energies (see **Table 2**). For the pristine GDY, the interaction remains exothermic, as indicated by the negative binding energy obtained.

Table 2. The binding energies (E_{bind} in eV) of all studied complexes in gas and water phase and solvation energy.

System	E_{bind} (eV)		
	Without BSSE correction	With BSSE correction	Presence of solvent
Tilted-OH	-0.23	-0.12	-0.095
Vertical-OH	-0.16	-0.06	-0.079
NH ₂ /F-oriented	-0.14	-0.01	-0.074
Hydroxyl-side	-0.26	-0.14	-0.108
Carbonyl-side	-0.20	-0.07	-0.113
FAV(N/O)-GDYNi	-4.41	-3.35	-2.926
FAV(N/O)-GDYCu	-3.96	-2.88	-2.928
FAV(N/O)-GDYTi	-5.79	-5.39	-2.696
FAV(N/OH)-GDYNi	-2.75	-2.00	-1.547
FAV(N/OH)-GDYCu	-2.74	-2.09	-1.926
FAV(N/OH)-GDYTi	-5.79	-5.45	-1.117

This confirms that the solvent does not suppress the intrinsic adsorption tendency of the pristine surface to interact with the adsorbate. However, once metal decoration is introduced, the binding energies become



more negative across all decorated configurations, demonstrating a clear enhancement in interaction strength and more stabilized adsorption process.

The thermodynamic parameters obtained in water further support the improvement introduced by metal decoration, as detailed in **Table 1**. For pristine GDY, the adsorption process exhibits a positive Gibbs free energy, including that the reaction is not spontaneous, even though the enthalpy change is slightly exothermic. The negative entropy values are consistent with the expected reduction in molecular freedom upon adsorption. Upon decoration, a clear shift in the thermodynamic behavior is observed. Gibbs free energy becomes negative for all decorated systems, demonstrating that adsorption becomes spontaneous under the same solvated conditions. Enthalpy values become more exothermic, providing the dominant contribution that drives the overall feasibility of the reaction. While entropy remains negative, enhanced enthalpic stabilization outweighs this contribution, yielding a thermodynamically favorable process.

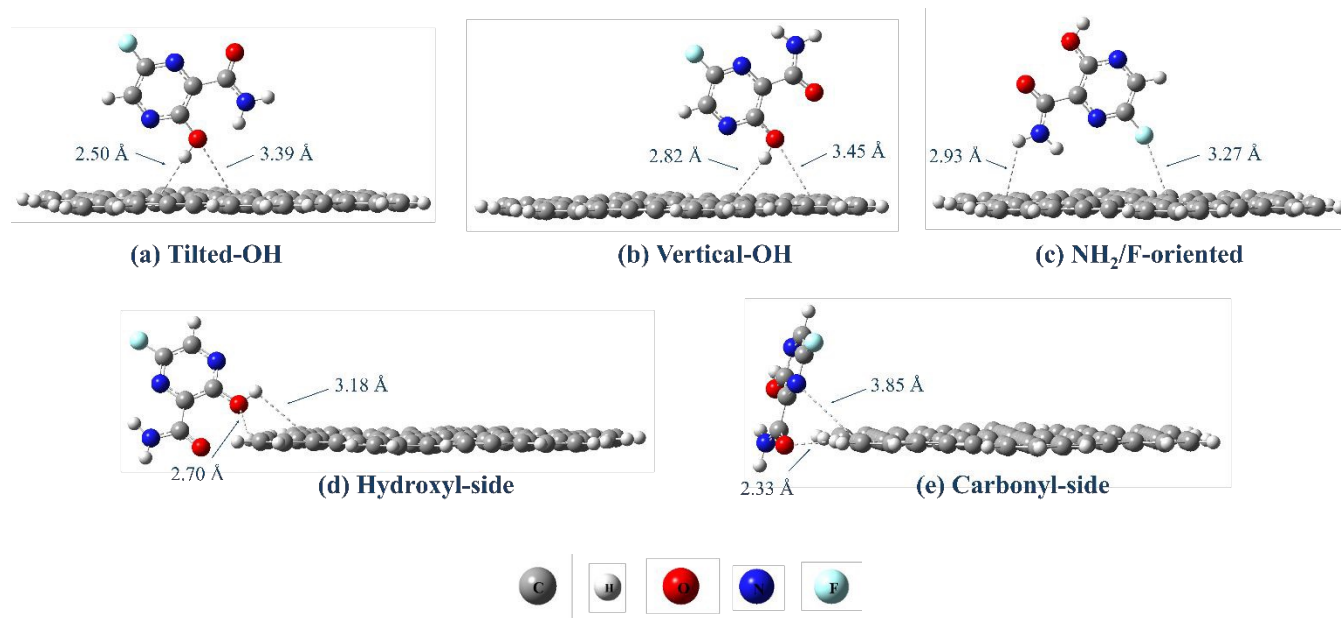


Figure. 9. Optimized geometries of FAV drug on GDY nanosheet in five orientations, with their interaction distances in solvent.



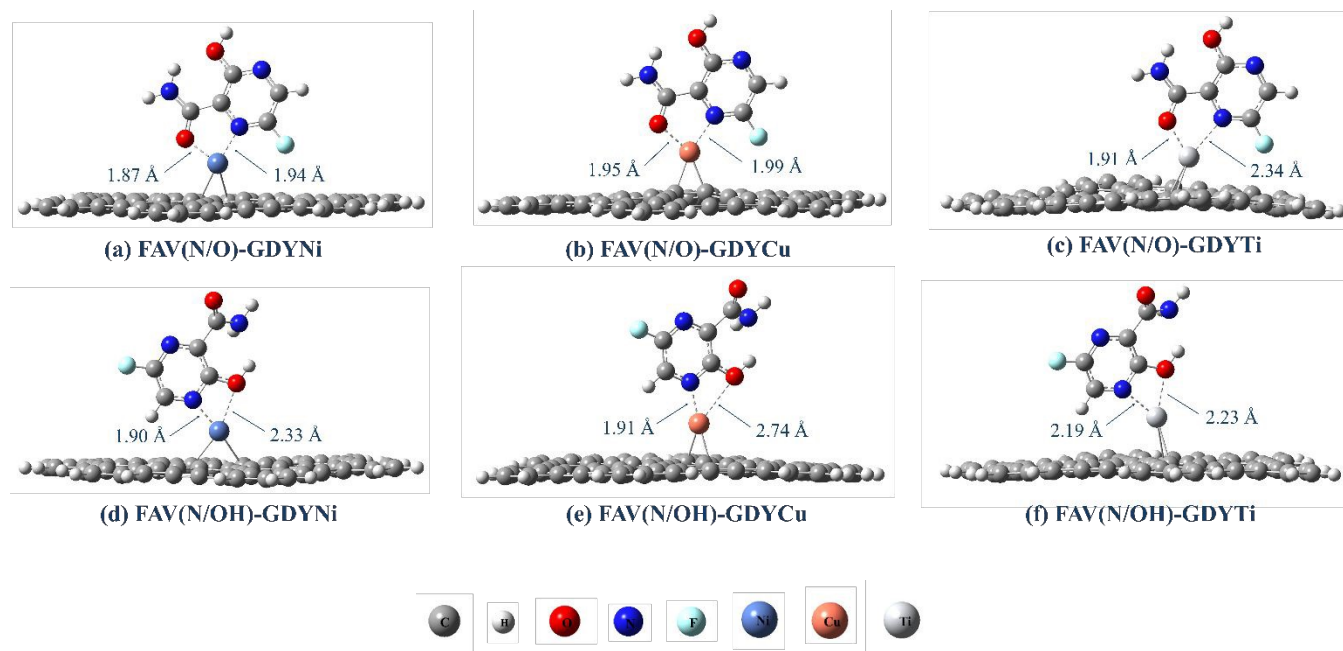


Figure 10. Optimized geometries for different adsorption orientations of FAV on decorated-GDY surfaces: Ni-GDY, Cu-GDY and Ti-GDY, with their interaction distances in solvent.

3.8. Global indices parameters

The set of global reactivity parameters presented in **Table 3**, including ionization potential (IP), electron affinity (EA), global hardness (η), softness (χ), chemical potential (μ), and electrophilicity index (ω) used to evaluate how the electronic structure of favipiravir response during adsorption. These descriptors help clarify the ability of molecules to donate or accept electrons (IP and EA), Its overall stability and resistance to electronic change (η and χ), and its tendency to attract electron density (μ and ω). Examining these parameters allows a clearer understanding of how the drug adjusts its electronic behavior in different orientations and when interacting with the modified GDY surface.

$$IP = -E_{HOMO} \quad (9)$$

$$EA = -E_{LUMO} \quad (10)$$

$$\eta = \frac{IP - EA}{2} \quad (11)$$

$$\chi = \frac{1}{\eta} \quad (12)$$



$$\mu_{ch} = \frac{IP + EA}{2} \quad (13)$$

$$\omega = \frac{\mu^2}{2\eta} \quad (14)$$

Table 3. The calculated values of ionization potential (IP), electron affinity (EA), global hardness (η), softness (χ), chemical potential (μ), and electrophilicity index (ω) for FAV with pristine and metal decorated GDY nanosheets.

System	IP (eV)	EA (eV)	η (eV)	χ (eV) ⁻¹	μ_{ch} (eV)	ω (eV)
Tilted-OH	5.378	2.879	1.249	0.800	-4.128	6.822
Vertical-OH	5.284	2.672	1.305	0.765	-3.978	6.061
NH₂/F-oriented	5.335	2.741	1.296	0.771	-4.038	6.286
Hydroxyl-side	5.149	2.539	1.304	0.766	-3.844	5.663
Carbonyl-side	5.182	2.605	1.288	0.775	-3.894	5.883
FAV(N/O)-GDYNi	9.829	9.015	0.406	2.45	-9.422	109.094
FAV(N/O)-GDYCu	9.598 ^α	8.066 ^α	0.765 ^α	1.305 ^α	-8.832 ^α	50.923 ^α
	9.568 ^β	8.549 ^β	0.509 ^β	1.962 ^β	-9.059 ^β	80.517 ^β
FAV(N/O)-GDYTi	14.412	14.083	0.164	6.079	-14.248	617.105
FAV(N/OH)-GDYNi	9.768	9.044	0.362	2.760	-9.406	122.107
FAV(N/OH)-GDYCu	9.917 ^α	7.757 ^α	1.079 ^α	0.925 ^α	8.837 ^α	36.159 ^α
	9.870 ^β	9.273 ^β	0.509 ^β	3.350 ^β	-9.572 ^β	153.48 ^β
FAV(N/OH)-GDYTi	14.264	13.919	0.172	5.801	-14.091	575.994

3.9. Natural bond orbital

The Natural Bond Orbital (NBO) analysis was performed to obtain a detailed description of the electronic interactions between favipiravir and GDY-nanosheet. This approach provides a quantitative description of electron delocalization through interactions between occupied Lewis-type orbitals (donors) and unoccupied non-Lewis's orbitals (acceptors). All NBO calculations were performed using density functional theory (DFT) at the B3LYP/6-31G(d) level of theory, which is well established for describing



orbital interactions and electronic delocalization. The interaction parameters, including the second-order perturbation stabilization energy ($E^{(2)}$), the energy difference between donor and acceptor orbitals ($E_j - E_i$), and the off-diagonal Fock matrix element F_{ij} , were evaluated to quantify the strength of donor-acceptor interactions. These parameters are summarized in **Table 4**.

The stabilization energy associated with each donor-acceptor interaction is estimated using second-order perturbation theory, expressed as:

$$E^{(2)} = q_i \frac{F_{ij}^2}{E_j - E_i} \quad (15)$$

where q_i is the occupancy of the donor orbital, E_i and E_j are the diagonal elements (orbital energies) of the donor and acceptor NBOs, respectively, and F_{ij} represents the off-diagonal Fock matrix element. Larger $E^{(2)}$ values indicate stronger donor-acceptor interactions and enhanced electronic stabilization of the complex. Among all investigated complexes, the strongest stabilization interaction is observed between LP (2) O and LP*(2) Ti in the FAV(N/O)-GDYTi complex, with a remarkably high stabilization energy of 71.79 kcal/mol, indicating pronounced charge delocalization and strong orbital overlap. Additionally, significant stabilization energies are found between LP (1) N and LP*(6) Ni interaction in the FAV(N/O)-GDYNi complexes, reaching values up to 69.46 kcal/mol, further confirming strong donor-acceptor coupling.

Table 4. Natural bond orbital analysis for the donor and acceptor interactions, as well as the second-order perturbation stabilization energy ($E^{(2)}$, kcal/mol), correspond to the charge transfer of FAV drug with pristine and metal decorated GDY nanosheets in gas phase.

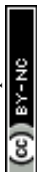
System	Donor NBO (i)	Acceptor NBO (j)	$E^{(2)}$ (kcal/mol)	$E_{(j)} - E_{(i)}$ a.u.	$F_{(i,j)}$ a.u.
Vertical OH	BD(3)C33- C57	BD*(1)C86 -O98	0.06	0.65	0.005
	BD(3)C22-C 32	LP*(1) H99	3.18	0.42	0.036
Tilted-OH	BD(3)C21-C55	BD*(1)C86-O98	0.05	0.67	0.005
	BD(3)C20-C 31	LP*(1) H99	0.83	0.41	0.018
NH₂/F- oriented	LP(1)N95	BD*(3)C21 - C55	0.08	0.36	0.005



	BD(3)C21-C55	BD*(1)N95-H96	0.50	0.77	0.018
Hydroxyl-side	BD(2)C59-C 78	LP*(1)H99	2.41	0.40	0.031
	LP(1)O98	BD*(1)C37-H 42	1.14	1.11	0.032
Carbonyl-side	LP(1)N90	BD*(1)C37-H 42	0.12	0.88	0.010
	LP(1)O94	BD*(1)C37-H 42	1.30	1.20	0.035
FAV(N/O)-GDYNi	LP(1)N91	LP*(6)Ni85	62.94	0.59	0.174
	LP(2)O95	LP*(6)Ni85	48.06	0.60	0.153
FAV(N/O)-GDYCu	LP(1)N90	LP*(6)Cu100	23.40	0.49	0.138
	LP(2)O94	LP*(6) Cu100	18.51	0.47	0.120
FAV(N/O)-GDYTi	LP(1)N91	LP*(4) Ti85	21.70	0.59	0.104
	LP(2)O95	LP*(2)Ti85	71.79	0.54	0.175
FAV(N/OH)-GDYNi	LP(1)N88	LP*(5)Ni85	69.46	0.56	0.177
	LP(1)O99	LP*(6)Ni85	12.61	0.89	0.095
FAV(N/OH)-GDYCu	LP(1)N87	LP*(6)Cu100	34.41	0.47	0.162
	LP(1) O98	LP*(7)Cu100	2.78	0.75	0.058
FAV(N/OH)-GDYTi	LP(1)N87	LP*(1) Ti 100	40.12	0.37	0.110
	LP(2)O98	LP*(3)Ti100	51.15	0.43	0.132

3.10. Work Function

The work function (ϕ) was evaluated to examine the effect of favipiravir adsorption on the electronic surface properties of GDY. This parameter is directly related to the minimum energy required to remove



an electron from the fermi level to the vacuum level and therefore provides useful insights into changes in surface electronic behavior upon interaction.

The work function was obtained using the relation:

$$\phi = V_{vac(\infty)} - E_F \quad (16)$$

where $V_{vac(\infty)}$ is the electrostatic potential at the vacuum level and E_F is the Fermi level of the system. Since the vacuum potential is defined at a position for the surface where the potential approaches zero, the work function can be approximated as the negative of the fermi energy, i.e., $\phi = -E_F$. The calculated values listed in table 4, show that the different favipiravir orientations on pristine exhibit relatively close work function values. After adsorption on decorated GDY, noticeable shifts in the Fermi energy are observed, which are directly reflected in the calculated work function values. These variations indicate that the interaction between favipiravir and the modified GDY surface alters the energy required for electron emission. Such changes in work function suggest a redistribution of electronic charge at the interface, which is a typical consequence of adsorption induced electronic coupling.

Additionally, the percentage change in work function was evaluated using the following equation:

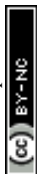
$$\% \Delta \phi = \frac{\phi_{complex} - \phi_{nanosheet}}{\phi_{nanosheet}} \times 100 \quad (17)$$

Where $\phi_{Complex}$ and $\phi_{nanosheet}$ represent the work functions of the adsorbed system and the pristine surface, respectively. This parameter provides a quantitative measure of how adsorption affects the surface electronic properties.

Overall, the observed changes in work function confirm that favipiravir adsorption induces measurable electronic modification at the GDY surface. These results highlight the importance of work function analysis in understanding surface electronic response upon interaction.

Table 5. The calculated values of HOMO energies (E_{HOMO}), LUMO energies (E_{LUMO}), energy gap (E_g) in eV and fermi level E_F in gas phase.

System	E_{HOMO}	E_{LUMO}	E_g	E_F (eV)	ϕ (eV)	$\Delta \phi$ (%)
Pristine	- 5.214	- 2.600	2.614	- 3.907	3.907	-



GDYNi	− 9.941	− 9.414	0.526	− 9.678	9.678	—
GDYCu	− 9.965 ^α	− 8.195 ^α	1.770 ^α	− 9.080 ^α	9.080 ^α	—
	− 9.893 ^β	− 9.337 ^β	0.555 ^β	− 9.615 ^β	9.615 ^β	
GDYTi	− 14.536	− 14.194	0.342	− 14.365	14.365	—
Tilted-OH	− 5.378	− 2.879	2.498	− 4.128	4.128	5.668
Vertical-OH	− 5.284	− 2.672	2.611	− 3.978	3.978	1.817
NH₂/F-oriented	− 5.335	− 2.741	2.593	− 4.038	4.038	3.342
Hydroxyl-side	− 5.149	− 2.539	2.609	− 3.844	3.844	− 1.615
Carbonyl-side	− 5.182	− 2.605	2.577	− 3.894	3.894	− 0.341
FAV(N/O)-GDYNi	− 9.829	− 9.015	0.813	− 9.422	9.422	− 2.638
FAV(N/O)-GDYCu	− 9.598 ^α	− 8.066 ^α	1.531 ^α	− 8.832 ^α	8.832 ^α	− 2.728 ^α
	− 9.568 ^β	− 8.549 ^β	1.019 ^β	− 9.059 ^β	9.059 ^β	− 5.782 ^β
FAV(N/O)-GDYTi	− 14.412	− 14.083	0.328	− 14.248	14.248	− 0.817
FAV(N/OH)-GDYNi	− 9.768	− 9.044	0.724	− 9.406	9.406	− 2.807
FAV(N/OH)-GDYCu	− 9.917 ^α	− 7.757 ^β	2.159 ^α	− 8.837 ^α	8.837 ^α	− 2.671 ^α
	− 9.870 ^α	− 9.273 ^β	0.596 ^β	− 9.572 ^β	9.572 ^β	− 0.448 ^β
FAV(N/OH)-GDYTi	− 14.264	− 13.919	0.344	− 14.091	14.091	− 1.906



3.11. Drug release mechanism

Controlled drug release at the target site is considered one of the most important requirements for an efficient drug delivery system, since it enhances the therapeutic performance of the drug while minimizing undesired side effects on healthy tissues. The relatively high adsorption energies obtained for the investigated complexes suggest strong interactions between Favipiravir and the metal-decorated GDY nanocarrier surface, which is beneficial for efficient drug loading and stabilization. Nevertheless, under physiological conditions, these interactions may become significantly weakened due to external factors such as solvent environment, temperature variations, and particularly acidic pH conditions, thereby facilitating controlled drug release. It is known that the pH of damaged or infected cells is lower than that of normal cells.

To evaluate the pH-responsive release behavior of Favipiravir from the GDY nanocarrier surface, a protonation approach was employed to simulate acidic physiological environments that may arise in intracellular compartments, where the pH is lower than neutral conditions. Such acidic environments are known to influence the protonation state of both drug molecules and nanocarrier surfaces, thereby affecting adsorption strength and facilitating controlled drug release. The effect of protonation on the adsorption was investigated by comparing the interaction distances and bond angles before and after protonation for FAV(N/O)-GDYNi, FAV(N/O)-GDYCu and FAV(N/O)-GDYTi complexes. Protonation was performed on the adsorption site and the nearest interacting atoms between Favipiravir and the decorated GDY surface (92). Following geometry optimization upon protonation, substantial structural changes were observed for three metal-decorated GDY loaded with the drug, Figure 11. Before the protonation, the neutral complexes exhibited shorter interaction distances together with bond angle closer to the ideal linear configuration (180°), indicating strong coordination interactions and effective orbital overlap between Favipiravir and the decorated GDY surfaces. However, after protonation, the adsorption distances become longer and the interaction angles deviated further away from 180° , reflecting distortion of the adsorption geometry and weakening of the coordination interaction.

For the FAV(N/O)-GDYNi complex in particular, the interaction distances increased, and thus weakened, from 1.89 Å and 1.92 Å before protonation to 2.16 Å and 2.01 Å after protonation. In addition, the C-O-Ni bond angle changed from 115.53° to 112.25° , while the C-N-Ni bond angle changed from 131.32° to 119.05° after protonation. Similarly, FAV(N/O)-GDYCu complex exhibits an interaction distance from 1.98 Å and 2.01 Å before protonation to 3.97 Å and 2.27 Å after protonation. In addition, the C-O-Cu



bond angle changed from 114.66° to 86.62° , whereas the C-N-Cu angle shifted from 129.39° to 95.15° after protonation. For the FAV(N/O)-GDYTi complex, the interaction distances changed from 1.98 Å and 2.26 Å before protonation to 2.24 Å and 2.19 Å after protonation. Furthermore, the C-O-Ti bond angle changed from 124.49 to 93.00° , while the C-N-Ti angle changed from 113.20 to 79.93° after protonation.

The deviation from linearity together with the elongation of the adsorption distances indicate reduced adsorption affinity and lower structural stability of the adsorbed configurations under acidic conditions. This has been further confirmed by obtaining positive binding energy reflecting unfavorable interaction. Consequently, protonation facilitates desorption and release of favipiravir from the GDY surfaces at the target acidic environment.

The obtained findings are consistent with previously reported theoretical investigations on related nanocarrier systems, where protonation under acidic conditions was found to reduce adsorption strength and facilitate drug desorption from carbon-based materials (93). Other reports also indicated that protonation transforms the interaction from strong adsorption to weaker noncovalent attraction accompanied by a noticeable increase in adsorption distance (94, 95). Additionally, several computational studies confirmed that protonation-induced weakening of adsorption interactions is generally associated with lower adsorption energies and enlarged drug-carrier separation distances under acidic conditions (96, 97). Overall, these results confirm that protonation under mildly acidic intracellular conditions effectively weakens the interaction between Favipiravir and the GDY nanocarrier surface, thereby facilitating drug desorption and supporting the feasibility of a pH-responsive drug delivery mechanism within the framework of density functional theory calculations.

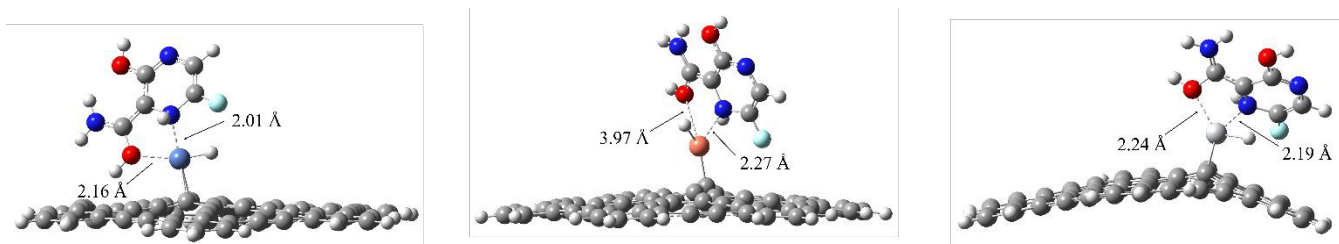


Figure 11. The optimized structures of protonated FAV(N/O)-GDYNi, FAV(N/O)-GDYCu and FAV(N/O)-GDYTi complexes in acidic environment.



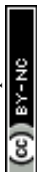
3.12. Comparison of binding energies (E_{bind}) and binding distances (d) of the FAV drug on pristine and metal decorated GDY nanosheets with other previously reported nanomaterials.

To evaluate the adsorption performance of favipiravir on pristine and decorated GDY, a comparative assessment performed against reported nanomaterials commonly investigated for drug delivery. This comparison focuses mainly on the calculated adsorption energies and binding distances, which collectively reflect the strength and stability of drug-nanocarrier interactions.

Pristine GDY demonstrates relatively weak adsorption strength, which aligns with the limited interaction capabilities typically reported for undoped carbon-based materials. Upon metal decoration, however, a substantial improvement is observed. All metal-decorated GDY exhibit markedly higher adsorption energies, indicating a more stable and favorable interaction compared with the numerous previously examined materials. This enhancement is consistently evident across the Ni, Cu and Ti modified surfaces, affirming the effectiveness of the decoration approach in reinforcing the adsorption behavior. Among the examined variants, Ti decoration provides the most pronounced improvement. These findings demonstrate that metal decoration particularly with Ti substantially enhances the adsorption performance of GDY when assessed against previously investigated nanomaterials.

Table 6. Comparison of binding energies (E_{bind}) and binding distances (d) of the FAV drug on pristine and metal decorated GDY nanosheets with other previously reported nanomaterials, respectively.

System	E_{bind} (eV)	d (Å)	Method	References
FAV				
GDY	-0.26	2.45 Å	B3LYP/6-31G(d)	Present work
GDYTi	-5.79	1.95 Å	B3LYP/6-31G(d)	Present work
GDYNi	-4.41	1.89 Å	B3LYP/6-31G(d)	Present work
GDYCu	-3.96	1.98 Å	B3LYP/6-31G(d)	Present work
C20	-0.17	3.45 Å	M062X/6-31G(d)/BSSE	(98)
C24	-0.085	3.355 Å	B3LYP/6-31G(d,p)	(99)
BNC	-3.469	1.45 Å	ω B97XD/6-31+G*/BSSE	(100)
GNS	-0.296	2.95 Å	PBE/USPP	(49)
BNNS	-0.70	3.43 Å	GGA-PBE/DNP	(101)

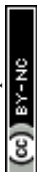


GYNT	-0.85	2.43 Å	B3LYP/6-31G(d)/LANL2DZ/BSSE	(50)
B12N12	-1.120	1.557 Å	B3LYP/6-31G(d,p)	(99)
C23B	-1.434	1.539 Å	B3LYP/6-31G(d,p)	(99)
CB11N12	-1.128	1.555 Å	B3LYP/6-31G(d,p)	(99)
Si-GYNT	-0.74	2.65 Å	6-31G(d)/LANL2DZ/BSSE	(50)
B3O3	-1.30	1.84 Å	ω B97XD/6-31+G(d,p)/BSSE	(102)
BN(Al)NS	-0.88	2.70 Å	GGA-PBE/DNP	(101)
C19Ni	-1.44	1.96 Å	ω B97XD/6-31+G(d,p)/BSSE	(51)
C19Ti	-1.59	2.05 Å	ω B97XD/6-31+G(d,p)/BSSE	(51)
C19Si	-1.88	1.80 Å	BSSE/M062X/6-31G(d)/BSSE	(98)
Be12O12	-1.31	1.67 Å	PBE/DNP	(103)
Mg12O12	-1.52	1.66 Å	PBE/DNP	(103)
Zn12O12	-0.51	1.70 Å	PBE/DNP	(103)
Ni-B12N12	-2.44	-	B3LYP/6-31 G(d,P)	(104)

4. Conclusion

In this work, density functional theory (DFT) calculations were employed to systematically investigate the adsorption behavior of favipiravir on pristine and transition metal-decorated graphdiyne (GDY) nanosheets to evaluate their suitability as efficient drug delivery platforms. The structural, energetic, electronic, and thermodynamic characteristics of the resulting drug-carrier complexes were examined in both gas and aqueous environments to assess their stability under idealized and physiologically relevant conditions.

The results demonstrate that pristine GDY exhibits relatively moderate interaction with favipiravir, whereas transition metal decoration significantly enhances the adsorption performance. This enhancement is reflected by larger binding energies, shorter interaction distances, and considerable charge transfer between favipiravir and the modified GDY surfaces. Among the investigated systems, FAV(N/O)-GDY_{Ni}, FAV(N/O)-GDY_{Cu}, and FAV(N/O)-GDY_{Ti} exhibited the strongest adsorption affinities,



highlighting the important role of metal decoration in tuning the electronic properties and adsorption capability of GDY nanosheets.

Comprehensive electronic analyses, including frontier molecular orbital analysis, density of states, natural bond orbital analysis, reduced density gradient–noncovalent interaction mapping, infrared spectral analysis, global reactivity descriptors, and work function calculations, consistently confirmed the strong interaction between favipiravir and the decorated GDY surfaces. The obtained results indicate that transition metal decoration effectively modulates the electronic structure of GDY, leading to enhanced stability and stronger drug–surface interactions. Thermodynamic calculations further revealed that the adsorption process becomes spontaneous and energetically favorable after metal decoration in both gas and solvent phases, confirming the stability of the investigated systems under realistic conditions.

To further examine the feasibility of controlled drug release, protonated models were investigated to simulate the mildly acidic intracellular environments, where nanocarrier-mediated drug release may occur after cellular internalization. The calculations showed that protonation substantially weakens the interaction between favipiravir and the metal-decorated GDY surface, resulting in reduced binding strength and increased separation distances. These findings suggest that efficient release of favipiravir remains achievable even for strongly adsorbed systems prior to protonation, supporting the pH-responsive behavior of the proposed nanocarriers.

Moreover, a detailed comparison of the optimized geometries and adsorption energies in vacuum and aqueous media revealed only minor changes, indicating that the investigated complexes maintain their structural stability and adsorption characteristics in solvent environments. This observation further supports the tolerance and applicability of the proposed systems under realistic physiological conditions. Overall, this theoretical study demonstrates that transition metal–decorated graphdiyne nanosheets represent promising nanocarriers for favipiravir delivery.

Author contribution

Mohamed M. Aboelnga: Supervision, Project administration, Validation, Computational analysis, Investigation, Conceptualization, Visualization, Formal analysis, Data curation, Software, Resources, Writing-review & editing. **Rana G. Elbayaa:** Writing-original draft, Visualization, Investigation, Formal analysis, Data curation, Investigation, Computational analysis, Methodology. **Elsayed Elbayoumy:**



Supervision, Validation, Conceptualization. **Marco Garavelli:** Formal analysis, Software, Resources, Writing-review & editing. **Mohsen Eltahawy:** Supervision, Validation, Conceptualization, Computational analysis, Investigation, Visualization, Formal analysis, Software, Resources.

Funding

This research did not receive any specific grant from funding agencies in the public, commercial, or not-for-profit sectors.

Declaration of Competing Interest

The authors declare that they have no known competing financial interests or personal relationships that could have appeared to influence the work reported in this paper.

Data availability

Data from this study will be made available from the corresponding author upon reasonable request.

Appendix A. Supplementary material

supplementary data to this article can be found online at

Author Information

Mohamed M. Aboelnga

Email: mohamed-aboelnga@du.edu.eg

Orcid: 0000-0002-3283-5884

Rana G. Elbayaa

Email: ranaelbayaa@students.du.edu.eg

Orcid: 0009-0004-1980-1307

Elsayed Elbayoumy:

Email: sayedelbayoumy@du.edu.eg

Orcid: 0000-0003-2634-8462

Marco Garavelli

Email: marco.garavelli@unibo.it

Orcid: <https://orcid.org/0000-0002-0796-289X>

Mohsen Eltahawy



Email: mohsen.eltahawy@sci.dmu.edu.eg

Orcid: 0000-0002-9561-9521

References:

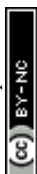
1. **Goldhill DH, Te Velthuis AJW, Fletcher RA, Langat P, Zambon M, Lackenby A, Barclay WS.** The mechanism of resistance to favipiravir in influenza. *Proc Natl Acad Sci U S A* 115: 11613–11618, 2018. doi: 10.1073/pnas.1811345115.
2. **Furuta Y, Gowen BB, Takahashi K, Shiraki K, Smee DF, Barnard DL.** Favipiravir (T-705), a novel viral RNA polymerase inhibitor. *Antiviral Res* 100: 446–454, 2013. doi: <https://doi.org/10.1016/j.antiviral.2013.09.015>.
3. **Goldhill DH, te Velthuis AJW, Fletcher RA, Langat P, Zambon M, Lackenby A, Barclay WS.** The mechanism of resistance to favipiravir in influenza. *Proceedings of the National Academy of Sciences* 115: 11613–11618, 2018. doi: 10.1073/pnas.1811345115.
4. **Furuta Y, Komeno T, Nakamura T.** Favipiravir (T-705), a broad spectrum inhibitor of viral RNA polymerase. *Proc. Jpn. Acad. Ser. B Phys. Biol. Sci.* 93 Japan Academy: 449–463, 2017.
5. **Wang M, Cao R, Zhang L, Yang X, Liu J, Xu M, Shi Z, Hu Z, Zhong W, Xiao G.** Remdesivir and chloroquine effectively inhibit the recently emerged novel coronavirus (2019-nCoV) in vitro. *Cell Res.* 30 Springer Nature: 269–271, 2020.
6. **De Clercq E.** New Nucleoside Analogues for the Treatment of Hemorrhagic Fever Virus Infections. *Chem. Asian J.* 14 John Wiley and Sons Ltd: 3962–3968, 2019.
7. **Rosenke K, Feldmann H, Westover JB, Hanley PW, Martellaro C, Feldmann F, Saturday G, Lovaglio J, Scott DP, Furuta Y, Komeno T, Gowen BB, Safronetz D.** Use of favipiravir to treat lassa virus infection in Macaques. *Emerg Infect Dis* 24: 1696–1699, 2018. doi: 10.3201/eid2409.180233.
8. **Oestereich L, Lüdtke A, Wurr S, Rieger T, Muñoz-Fontela C, Günther S.** Successful treatment of advanced Ebola virus infection with T-705 (favipiravir) in a small animal model. *Antiviral Res* 105: 17–21, 2014. doi: <https://doi.org/10.1016/j.antiviral.2014.02.014>.
9. **Arab-Zozani M, Hassanipour S, Ghoddoosi-Nejad D.** Favipiravir for treating patients with novel coronavirus (COVID-19): Protocol for a systematic review and meta-analysis of randomised clinical trials. *BMJ Open* 10, 2020. doi: 10.1136/bmjopen-2020-039730.



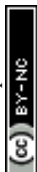
10. **Agrawal U, Raju R, Udwardia ZF.** Favipiravir: A new and emerging antiviral option in COVID-19. *Med. J. Armed Forces India* 76 Elsevier B.V.: 370–376, 2020.
11. **McKee DL, Sternberg A, Stange U, Laufer S, Naujokat C.** Candidate drugs against SARS-CoV-2 and COVID-19. *Pharmacol. Res.* 157 Academic Press: 2020.
12. **Ahusayni K, Alharthi S, Alhazmi M, Alaithan S, Alotaibi Y, Alhaddad Z, Alrowaished A, Almousa H, Hakami A, Alotaibi Y.** Safety and efficacy of favipiravir in COVID-19: a comprehensive literature review. .
13. **Yanai H.** Favipiravir: A possible pharmaceutical treatment for COVID-19. *J. Endocrinol. Metab.* 10 Elmer Press: 33–34, 2020.
14. **Hirouchi T, Ota S, Mashima D, Boku R, Yoshida Y, Iwata K, Shinada K, Matsumoto T, Morikawa M, Sato T, Shinoda M, Kamachi K, Shinkai M.** A case of COVID-19 pneumonia successfully treated with favipiravir (Avigan) in which serum SARS-CoV-2 RNA detected by LAMP method was clinically useful. *Journal of Infection and Chemotherapy* 27: 379–383, 2021. doi: 10.1016/j.jiac.2020.10.011.
15. **Rad AS, Ardjmand M, Esfahani MR, Khodashenas B.** DFT calculations towards the geometry optimization, electronic structure, infrared spectroscopy and UV–vis analyses of Favipiravir adsorption on the first-row transition metals doped fullerenes; a new strategy for COVID-19 therapy. *Spectrochim Acta A Mol Biomol Spectrosc* 247, 2021. doi: 10.1016/j.saa.2020.119082.
16. **De Clercq E.** New Nucleoside Analogues for the Treatment of Hemorrhagic Fever Virus Infections. *Chem. Asian J.* 14 John Wiley and Sons Ltd: 3962–3968, 2019.
17. **Ergür FÖ, Yıldız M, Şener MU, Kavurgacı S, Ozturk A.** Adverse effects associated with favipiravir in patients with COVID-19 pneumonia: a retrospective study. *Sao Paulo Medical Journal* 140: 372–377, 2022. doi: 10.1590/1516-3180.2021.0489.R1.13082021.
18. **Tariq A, Nazir S, Arshad AW, Nawaz F, Ayub K, Iqbal J.** DFT study of the therapeutic potential of phosphorene as a new drug-delivery system to treat cancer. *RSC Adv* 9: 24325–24332, 2019. doi: 10.1039/c9ra02778e.
19. **Jiang L, Li L, He X, Yi Q, He B, Cao J, Pan W, Gu Z.** Overcoming drug-resistant lung cancer by paclitaxel loaded dual-functional liposomes with mitochondria targeting and pH-response. *Biomaterials* 52: 126–139, 2015. doi: 10.1016/j.biomaterials.2015.02.004.
20. **Qiu L, Chen T, Öçsoy I, Yasun E, Wu C, Zhu G, You M, Han D, Jiang J, Yu R, Tan W.** A cell-targeted, size-photocontrollable, nuclear-uptake nanodrug delivery system for drug-resistant cancer therapy. *Nano Lett* 15: 457–463, 2015. doi: 10.1021/nl503777s.



21. **Gallo M, Favila A, Glossman-Mitnik D.** DFT studies of functionalized carbon nanotubes and fullerenes as nanovectors for drug delivery of antitubercular compounds. *Chem Phys Lett* 447: 105–109, 2007. doi: <https://doi.org/10.1016/j.cplett.2007.08.098>.
22. **Alipour E, Alimohammady F, Yumashev A, Maselena A.** Fullerene C60 containing porphyrin-like metal center as drug delivery system for ibuprofen drug. *J Mol Model* 26, 2020. doi: 10.1007/s00894-019-4267-1.
23. **Hazrati MK, Hadipour NL.** Adsorption behavior of 5-fluorouracil on pristine, B-, Si-, and Al-doped C60 fullerenes: A first-principles study. *Phys Lett A* 380: 937–941, 2016. doi: <https://doi.org/10.1016/j.physleta.2016.01.020>.
24. **Parlak C, Alver Ö, Şenyel M.** Computational study on favipiravir adsorption onto undoped- and silicon-decorated C60 fullerenes. *J Theor Comput Chem* 16: 1750011, 2017. doi: 10.1142/S0219633617500110.
25. **Son KH, Hong JH, Lee JW.** Carbon nanotubes as cancer therapeutic carriers and mediators [Online]. *Int J Nanomedicine* 11: 5163–5185, 2016. <https://api.semanticscholar.org/CorpusID:6256474>.
26. **Xue Z, Zhu M, Dong Y, Feng T, Chen Z, Feng Y, Shan Z, Xu J, Meng S.** An integrated targeting drug delivery system based on the hybridization of graphdiyne and MOFs for visualized cancer therapy. *Nanoscale* 11: 11709–11718, 2019. doi: 10.1039/C9NR02017A.
27. **Chu S, Shi X, Tian Y, Gao F.** pH-Responsive Polymer Nanomaterials for Tumor Therapy. *Front. Oncol.* 12 Frontiers Media S.A.: 2022.
28. **Li X, Jiang H, He N, Yuan WE, Qian Y, Ouyang Y.** Graphdiyne-Related Materials in Biomedical Applications and Their Potential in Peripheral Nerve Tissue Engineering. *Cyborg and Bionic Systems* 2022 American Association for the Advancement of Science: 2022.
29. **Jia Z, Li Y, Zuo Z, Liu H, Huang C, Li Y.** Synthesis and Properties of 2D Carbon-Graphdiyne. [Online]. *Acc Chem Res* 50 10: 2470–2478, 2017. <https://api.semanticscholar.org/CorpusID:206382999>.
30. **Gao X, Liu H, Wang D, Zhang J.** Graphdiyne: Synthesis, properties, and applications. *Chem. Soc. Rev.* 48 Royal Society of Chemistry: 908–936, 2019.
31. **Wang Z, Wang H, Zhang X, Yuan Y, Wang L, Liu J, Chen C.** Graphdiyne-based nanomaterials: Synthesis, properties, and biomedical applications. *ChemPhysMater* 4 KeAi Communications Co.: 207–233, 2025.



32. **Eatemadi A, Daraee H, Karimkhanloo H, Kouhi M, Zarghami N, Akbarzadeh A, Abasi M, Hanifehpour Y, Joo SW.** Carbon nanotubes: Properties, synthesis, purification, and medical applications. *Nanoscale Res Lett* 9: 1–13, 2014. doi: 10.1186/1556-276X-9-393.
33. **Rhazouani A, Gamrani H, El Achaby M, Aziz K, Gebrati L, Uddin MS, Aziz F.** Synthesis and Toxicity of Graphene Oxide Nanoparticles: A Literature Review of in Vitro and in Vivo Studies. *Biomed Res. Int.* 2021 Hindawi Limited: 2021.
34. **Zhang W, Zhang Z, Zhang Y.** The application of carbon nanotubes in target drug delivery systems for cancer therapies. *Nanoscale Res. Lett.* 6: 1–22, 2011.
35. **Zhao L-X, Fan Y-G, Zhang X, Li C, Cheng X-Y, Guo F, Wang Z-Y.** Graphdiyne biomaterials: from characterization to properties and applications. *J Nanobiotechnology* 23: 169, 2025. doi: 10.1186/s12951-025-03227-y.
36. **Kadhim MM, Taha A, Mahal RK, Hachim SK, Abdullaha SA, Rheima AM.** Molecular modeling for sensing of cisplatin drug by graphdiyne: electronic study via DFT. *J Mol Model* 29, 2023. doi: 10.1007/s00894-023-05511-w.
37. **Nagarajan V, Chandiramouli R.** Flutamide drug interaction studies on graphdiyne nanotube – A first-principles study. *Comput Theor Chem* 1167: 112590, 2019. doi: <https://doi.org/10.1016/j.comptc.2019.112590>.
38. **Srimathi U, Nagarajan V, Chandiramouli R.** Interaction of Imuran, Pentasa and Hyoscyamine drugs and solvent effects on graphdiyne nanotube as a drug delivery system - A DFT study. *J Mol Liq* 265: 199–207, 2018. doi: <https://doi.org/10.1016/j.molliq.2018.05.114>.
39. **Xu P, Na N, Mohamadi A.** Investigation the application of pristine graphdiyne (GDY) and boron-doped graphdiyne (BGDY) as an electronic sensor for detection of anticancer drug. *Comput Theor Chem* 1190: 112996, 2020. doi: <https://doi.org/10.1016/j.comptc.2020.112996>.
40. **Tabandeh Z, Reisi-Vanani A.** Investigation of the adsorption behavior of two anticancer drugs on the pristine and BN-doped graphdiyne nanosheet: A DFT-D3 perception. *Diam Relat Mater* 119: 108564, 2021. doi: <https://doi.org/10.1016/j.diamond.2021.108564>.
41. **Pallikkara Chandrasekharan S, Lakshmy S, Sanyal G, Kalarikkal N, Trivedi R, Chakraborty B.** Metal-decorated γ -graphyne as a drug transporting agent for the mercaptopurine chemotherapy drug: a DFT study. *Phys Chem Chem Phys* 25: 9461–9471, 2023. doi: 10.1039/D2CP05379A.
42. **Shen Z, Nieh M, Li Y.** Decorating Nanoparticle Surface for Targeted Drug Delivery: Opportunities and Challenges [Online]. *Polymers (Basel)* 8, 2016. <https://api.semanticscholar.org/CorpusID:13789594>.



43. **Ahmed Y, Ahmed AT, Mustafa MA, Kakkad A, Ballal S, Kalia R, Kubaev A, Arya R, Ibraheem AY, Bekit M, Naglah AM.** Anti-cancer chlorambucil drug delivery by Pt, au, and Ir-decorated ZnO nanotubes. *Solid State Commun* 403: 115972, 2025. doi: <https://doi.org/10.1016/j.ssc.2025.115972>.
44. **Saadh MJ, Abdalkareem Jasim S, Mahal A, Cáceres OV, Curay Yaulema CS, Obaidullah AJ, Abed Jawad M, Abdali Abdulridui H, Zainul R.** Sc-decorated GaN nanotube vehicle for 5-fluorouracil anti-cancer drug delivery: A computational study. *Comput Theor Chem* 1239: 114745, 2024. doi: <https://doi.org/10.1016/j.comptc.2024.114745>.
45. **Kadhim MM, Abdullaha SA, Zedan Taban T, Ahmed Hamza T, Mahdi Rheima A, Hachim SK.** Application of pure and Ti-decorated AIP nano-sheet in the dacarbazine anti-cancer drug delivery: DFT calculations. *Comput Theor Chem* 1220: 113999, 2023. doi: <https://doi.org/10.1016/j.comptc.2022.113999>.
46. **Asadi L, Salehpour M, Saadati Z, Joata Bayrami A.** Transition metal-decorated MgO nanocages as drug carriers for the chlormethine drug. *Comput Theor Chem* 1236: 114618, 2024. doi: <https://doi.org/10.1016/j.comptc.2024.114618>.
47. **Souri M.** Investigation of nonlinear optical properties of a group of transition metal-decorated B12N12 nanocages: A DFT study. *Physica B Condens Matter* 676: 415665, 2024. doi: <https://doi.org/10.1016/j.physb.2024.415665>.
48. **Souri M.** Decorated BN nanocones as NLO-active nanocarriers of nitrosoarea anticancer drug: A DFT study. *Comput Theor Chem* 1253: 115423, 2025. doi: <https://doi.org/10.1016/j.comptc.2025.115423>.
49. **Ibrahim MAA, Hamad MHA, Mahmoud AHM, Mekhemer GAH, Sidhom PA, Sayed SRM, Moussa NAM, Rabee AIM, Dabbish E, Shoeib T.** Adsorption of Favipiravir on pristine graphene nanosheets as a drug delivery system: a DFT study. *RSC Adv* 13: 17465–17475, 2023. doi: [10.1039/d3ra03227b](https://doi.org/10.1039/d3ra03227b).
50. **Asgari MA, Bahmani N.** Synergistic effect of Si-doping and Fe2O3-encapsulation on drug delivery and sensor applications of γ -graphyne nanotube toward favipiravir as an antiviral for COVID-19: A DFT study. *Journal of the Indian Chemical Society* 99, 2022. doi: [10.1016/j.jics.2022.100666](https://doi.org/10.1016/j.jics.2022.100666).
51. **Rad AS, Ardjmand M, Esfahani MR, Khodashenas B.** DFT calculations towards the geometry optimization, electronic structure, infrared spectroscopy and UV–vis analyses of Favipiravir adsorption on the first-row transition metals doped fullerenes; a new strategy for COVID-19 therapy. *Spectrochim Acta A Mol Biomol Spectrosc* 247, 2021. doi: [10.1016/j.saa.2020.119082](https://doi.org/10.1016/j.saa.2020.119082).



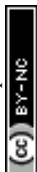
52. **Zoberbier T, Chamberlain TW, Biskupek J, Kuganathan N, Eyhusen S, Bichoutskaia E, Kaiser U, Khlobystov AN.** Interactions and reactions of transition metal clusters with the interior of single-walled carbon nanotubes imaged at the atomic scale. [Online]. *J Am Chem Soc* 134 6: 3073–9, 2012. <https://api.semanticscholar.org/CorpusID:14749833>.
53. **Mashhadzadeh AH, Vahedi AM, Ardjmand M, Ahangari MG.** Investigation of heavy metal atoms adsorption onto graphene and graphdiyne surface: A density functional theory study. *Superlattices Microstruct* 100: 1094–1102, 2016. doi: <https://doi.org/10.1016/j.spmi.2016.10.079>.
54. **Teleb NH, Sakr MAS, Abd-Elkader OH, Abdelsalam H, Zhang Q.** Exploring the impact of metal doping on drug delivery efficiency in g-C₃N₄ systems. *Comput Theor Chem* 1251: 115338, 2025. doi: <https://doi.org/10.1016/j.comptc.2025.115338>.
55. **Rad AS, Aghaei SM, Aali E, Peyravi M.** Study on the electronic structure of Cr- and Ni-doped fullerenes upon adsorption of adenine: A comprehensive DFT calculation. *Diam Relat Mater* 77: 116–121, 2017. doi: <https://doi.org/10.1016/j.diamond.2017.06.013>.
56. **Saadh MJ, Ayesb AI, El-Muraikhi MD, Dhiaa SM, Shomurotova S, Ahmadi TS, Mirzaei M, Da'i M, Ghotekar S, Ibrahim MA, Salem-Bekhit MM.** Structural and electronic assessments of Thiamazole adsorption on the transition metal doped fullerenes as a potential smart drug delivery platform. *Physica B Condens Matter* 685: 416006, 2024. doi: <https://doi.org/10.1016/j.physb.2024.416006>.
57. **Acosta-García A, Rodriguez-Leon AI, Santamaria R.** Transition-metal doped C60 fullerene for temozolomide anticancer drug delivery: A theoretical study. *Diam Relat Mater* 164: 113493, 2026. doi: <https://doi.org/10.1016/j.diamond.2026.113493>.
58. **Guan H, Sun H, Zhao X.** Application of Density Functional Theory to Molecular Engineering of Pharmaceutical Formulations [Online]. *Int J Mol Sci* 26, 2025. <https://api.semanticscholar.org/CorpusID:277533221>.
59. **Zamani A, Khelef A, Patel P, Ezhilarasan G, Ansar K, SINGLA S, Sahu BN, Shah SK, SasiKiran P.** Computational insights into B12N12 nanocage as a promising carrier for mesalazine delivery: a DFT study. *Comput Biol Chem* 119: 108585, 2025. doi: <https://doi.org/10.1016/j.compbiolchem.2025.108585>.
60. **Jouonang Létché G, Tamafo Fouegue AD, de Paul Zoua V, Abdoul Ntieche R, Noumi GB.** DFT investigation of the adsorption and sensing ability of pure, Al and Ca-doped B12N12 nanocages toward thalidomide drug. *Mater Sci Semicond Process* 185: 108980, 2025. doi: <https://doi.org/10.1016/j.mssp.2024.108980>.



61. **Saadh MJ, Jasim SA, Dhiaa SM, Chandra S, Alwan HA, Baeissa HM, Omran AA, Kamal M, Kadhum EH.** A DFT study the role of pristine and metal doped of g-CN nanosheet for drug delivery system. *Comput Theor Chem* 1232: 114448, 2024. doi: <https://doi.org/10.1016/j.comptc.2023.114448>.
62. **Rizwan HA, Khan MU, Anwar A, Khan MU, Sohail A, Ahmed S, Alshehri SM.** Deciphering the adsorption and sensing performance of Al₂₄N₂₄ and B₂₄N₂₄ nanoclusters as a drug delivery system for nitrosourea anticancer drug: A DFT insight. *Surfaces and Interfaces* 51: 104779, 2024. doi: <https://doi.org/10.1016/j.surfin.2024.104779>.
63. **Sarfaraz S, Yar M, Sohaib M, Umair Ashraf M, Ayub K.** Cavitations based nanocapsule as smart and highly effective vehicle for 5-fluorouracil anti-cancer drug delivery: DFT insights. *J Mol Liq* 399: 124436, 2024. doi: <https://doi.org/10.1016/j.molliq.2024.124436>.
64. **Nikfar Z, Shariatnia Z.** DFT computational study on the phosphate functionalized SWCNTs as efficient drug delivery systems for anti-osteoporosis zoledronate and risedronate drugs. *Physica E Low Dimens Syst Nanostruct* 91: 41–59, 2017. doi: <https://doi.org/10.1016/j.physe.2017.04.011>.
65. **Xu H, Li L, Fan G, Chu X.** DFT study of nanotubes as the drug delivery vehicles of Efavirenz. *Comput Theor Chem* 1131: 57–68, 2018. doi: <https://doi.org/10.1016/j.comptc.2018.03.032>.
66. **Becke AD.** Density-functional exchange-energy approximation with correct asymptotic behavior. *Phys Rev A (Coll Park)* 38: 3098, 1988.
67. **Frisch M, Trucks GW, Schlegel HB, Scuseria GE, Robb MA, Cheeseman JR, Scalmani G, Barone V, Mennucci B, Petersson GA.** gaussian 09, Gaussian. Inc, Wallingford CT 121: 150–166, 2009.
68. **Ibrahim MAA, Rady ASM, Sidhom PA, Soliman MES, Khan S, El-Tayeb MA, Abdelbacki AMM, Shoeib T, Mohamed LA.** A comparative DFT study of beryllium oxide (Be₁₂O₁₂) and boron nitride (B₁₂N₁₂) nanocages as potent drug delivery systems for allopurinol drug. *Chem Phys Lett* 857: 141729, 2024. doi: <https://doi.org/10.1016/j.cplett.2024.141729>.
69. **Ahmed U, Reshak AH, Abbass NM, Khan AA, Khan SA, Sajjad A, Ayub M, Ali D, Ramli MM.** Exploring the adsorption of 5-fluricil anticancer drug over the Zn₁₂S₁₂ nanostructure as a drug delivery system: DFT study. *Chinese Journal of Physics* 96: 219–227, 2025. doi: <https://doi.org/10.1016/j.cjph.2025.01.034>.
70. **Rizehbandi M, Davoodi F, Ghasemi M, Javanshir S.** Comprehensive theoretical analysis of gabapentin antiepileptic adsorption on pristine and Al-doped boron nitride nanotubes surface as a drug delivery vehicle: A DFT study. *Comput Theor Chem* 1252: 115381, 2025. doi: <https://doi.org/10.1016/j.comptc.2025.115381>.



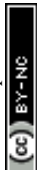
71. **Perveen M, Noreen L, Waqas M, Mehmood RF, Iqbal J, Manzoor S, Nazir S, Shawky AM, Khera RA.** A DFT approach for finding therapeutic potential of graphyne as a nanocarrier in the doxorubicin drug delivery to treat cancer. *J Mol Graph Model* 124: 108537, 2023. doi: <https://doi.org/10.1016/j.jmngm.2023.108537>.
72. **Ibrahim MAA, Mahmoud AHH, Rady ASM, Mohamed LA, Khan S, Rady A.** Unravelling the potential of zinc oxide (ZnO) as a drug delivery system for 5-Aminolevulinic acid drug: Insights from DFT calculations. .
73. **Chen C, Guo L, Luo Y, Zuo K, Tang D.** DFT insight into M@B40 (M = Au, Ag, Cu, Zn, Pt) metal-borospherene as melphalan anticancer drug nanocarriers. .
74. **Hsu C-Y, Mirzaei M.** Adsorption of Cycloserine (Seromycin) onto a beryllium oxide nanocage for assessing a potential drug carrier scaffold along with DFT computations. *Comput Theor Chem* 1251: 115317, 2025. doi: <https://doi.org/10.1016/j.comptc.2025.115317>.
75. **Chou-Yi H, Abdulrazzaq Mutar A, Ameer AJ, Kadhim MM, Ahmed Hamza T, ALSailawi HA, Altimari US, Alawadi A, Alsalamy A.** Exploring boron nitride nanostructures for effective pyrazinamide drug delivery: A DFT study. *Comput Theor Chem* 1230: 114378, 2023. doi: <https://doi.org/10.1016/j.comptc.2023.114378>.
76. **Abinaya V, Janani Sivasankar K, Sneha J, John Thiruvadigal D.** Organic acid-functionalized Aluminum Nitride Nanotubes (AlNNT) for targeted drug delivery using Carmustine: A DFT study. *Surfaces and Interfaces* 64: 106438, 2025. doi: <https://doi.org/10.1016/j.surfin.2025.106438>.
77. **Sadeghi M, Khoshnevisan B.** DFT study of Ti3C2 MXene nanosheets as a drug delivery system for 5-fluorouracil††Electronic supplementary information (ESI) available. See DOI: <https://doi.org/10.1039/d4ra02399d>. *RSC Adv* 14: 20300–20311, 2024. doi: <https://doi.org/10.1039/d4ra02399d>.
78. **Opi MH, Ahmed T, Swarna MR, Piya AA, Shamim SUD.** Assessment of the drug delivery potential of graphene, boron nitride and their in-plane doped structures for hydroxyurea anti-cancer drug via DFT study. *Nanoscale Adv* 6: 5042–5054, 2024. doi: <https://doi.org/10.1039/d4na00428k>.
79. **Bin Jordan YA, Bakr RA, Kumar A, Renuka Jyothi S, Singh M, Nathiya D, Kundlas M, Siva Prasad G V, Bekhit MM, Rusho MA.** Computational investigation of drug delivery through pristine and Al/Ga-doped carbon nitride nanomaterials. *Mater Chem Phys* 345: 131231, 2025. doi: <https://doi.org/10.1016/j.matchemphys.2025.131231>.



80. **Gharelar SA, Masoudi S, Masnabadi N, Ghasemi MH.** Comparison of the adsorption behavior of melphalan anti-cancer drug on MgS nano-cage: A DFT study. *Results Chem* 15: 102273, 2025. doi: <https://doi.org/10.1016/j.rechem.2025.102273>.
81. **Aboelnga MM, Seliem MM, El-Bayoumy E, El-Tahawy M.** DFT investigation of dye adsorption on pristine and doped graphdiyne: toward efficient removal of disperse yellow 3 from wastewater. *Nanoscale Adv* 7: 7363–7381, 2025. doi: [10.1039/d5na00720h](https://doi.org/10.1039/d5na00720h).
82. **Helal MW, Ezzat AA, Kamal FAM, Aboelnga MM.** Tailoring CO₂ capture in C₃₀ fullerenes by titanium doping: A comprehensive DFT study. *Sep Purif Technol* 395: 137744, 2026. doi: <https://doi.org/10.1016/j.seppur.2026.137744>.
83. **Attallah MI, Aboelnga MM.** Comparative DFT investigation of pristine and Cu-decorated MgO Nanorings as promising sensors for hazardous gases CO, HCN, and PH₃. *Sep Purif Technol* 395: 137637, 2026. doi: <https://doi.org/10.1016/j.seppur.2026.137637>.
84. **Ragab SM, Moawed EA, Elsadda RR, Khairy GM, Aboelnga MM.** Tuning Al₉N₉ nanoring for sensing and removal of chemical warfare agents via copper decoration: Insights from DFT calculations. *Surfaces and Interfaces* 81: 108426, 2026. doi: <https://doi.org/10.1016/j.surfin.2026.108426>.
85. **Lotfy S, Elbayoumy E, Moawed EA, Aboelnga MM.** Atomistic insights into MgO nanoring as an efficient drug sensor for amphetamine derivatives. *J Mol Liq* 436, 2025. doi: [10.1016/j.molliq.2025.128256](https://doi.org/10.1016/j.molliq.2025.128256).
86. **Rizwan HA, Khan MU, Anwar A, Idrees M, Siddiqui NA.** A molecular modeling study of pristine and Li-doped B₁₆N₁₆ nanocages for sensing G-series nerve agents using DFT-D3. *J Mol Graph Model* 139: 109069, 2025. doi: <https://doi.org/10.1016/j.jmgm.2025.109069>.
87. **Liaqat M, Javed M, Ahmad A, Yaqoob J, Hassan AU, Siddiqui NA, Khan MU.** Advanced Detection and Electrochemical Sensing of Hazardous Short-Branched Phthalate Plasticizers Using Novel Ga₁₂N₁₂ Nanomaterials: A DFT Study. *J Inorg Organomet Polym Mater* 35: 1219–1239, 2025. doi: [10.1007/s10904-024-03366-z](https://doi.org/10.1007/s10904-024-03366-z).
88. **Ishtiaq M, Khan MU, Liaqat M, Idrees M, El-Tayeb MA, Ibrahim MAA.** Unveiling the Carbon Nitride (C₂₄ N₂₄) Nanocage as a Rapid and Selective Electrochemical Sensor for Chemotherapeutic Agents Hydroxyurea and Nitrosourea: A DFT Study. *Journal of Computational Biophysics and Chemistry* 24: 1099–1119, 2025. doi: [10.1142/S2737416525500127](https://doi.org/10.1142/S2737416525500127).
89. **Rizwan HA, Khan MU, Anwar A, Alharthi S, Amin MA.** First theoretical framework of Al₉N₉ and B₉N₉ nanorings for unveiling their unique detection and sensing potential for SF₆



- decomposition gases (H₂S, SO₂, SOF₂, and SO₂F₂): toward real-time gas sensing in high-voltage power systems. *RSC Adv* 15: 20020–20039, 2025. doi: 10.1039/D5RA03312H.
90. **Al-Shaalan NH, Rizwan HA, Khan MU, Anwar A, Ishtiaq M, Amin MA.** Structural and energetic evaluation of boron carbide (B₁₆C₁₆) nanocage as a sensing material for A-series nerve agents: a DFT study. *Struct Chem* 37: 185–207, 2026. doi: 10.1007/s11224-025-02522-6.
91. **Alotaibi MM, Rizwan HA, Khan MU.** Al₁₂C₁₂ and B₁₂C₁₂ Nanocages as High-Performance Reversible Sensors for Real-Time Detection of Toxic Cyanide Gases for Industrial and Environmental Safety: A DFT Perspective. .
92. **Hazrati MK, Javanshir Z, Bagheri Z.** B₂₄N₂₄ fullerene as a carrier for 5-fluorouracil anti-cancer drug delivery: DFT studies. *J Mol Graph Model* 77: 17–24, 2017. doi: 10.1016/j.jmgm.2017.08.003.
93. **Esfahani MD, Khan AA.** Alkali metal decorated C₆₀fullerenes as promising materials for delivery of the 5-fluorouracil anticancer drug: A DFT approach. *RSC Adv* 12: 3948–3956, 2022. doi: 10.1039/d1ra09153k.
94. **Alkhalifah MA, Yar M, Bayach I, Sheikh NS, Ayub K.** Covalent Organic Framework (C₆N₆) as a Drug Delivery Platform for Fluorouracil to Treat Cancerous Cells: A DFT Study. *Materials* 15, 2022. doi: 10.3390/ma15217425.
95. **Hosseini A, Vessally E, Yahyaei S, Edjlali L, Bekhradnia A.** A Density Functional Theory Study on the Interaction Between 5-Fluorouracil Drug and C₂₄ Fullerene. *J Clust Sci* 28: 2681–2692, 2017. doi: 10.1007/s10876-017-1253-6.
96. **Alipour E, Alimohammady F, Yumashev A, Maselena A.** Fullerene C₆₀ containing porphyrin-like metal center as drug delivery system for ibuprofen drug. *J Mol Model* 26, 2020. doi: 10.1007/s00894-019-4267-1.
97. **Hazrati MK, Bagheri Z, Bodaghi A.** Application of C₃₀B₁₅N₁₅ heterofullerene in the isoniazid drug delivery: DFT studies. *Physica E Low Dimens Syst Nanostruct* 89: 72–76, 2017. doi: 10.1016/j.physe.2017.02.009.
98. **Alver Ö, Parlak C, Umar Y, Ramasami P.** DFT/QTAIM analysis of favipiravir adsorption on pristine and silicon doped C₂₀ fullerenes. *Main Group Metal Chemistry* 42: 143–149, 2019. doi: 10.1515/mgmc-2019-0016.
99. **Soliman KA, Aal SA.** Theoretical investigation of favipiravir antiviral drug based on fullerene and boron nitride nanocages. *Diam Relat Mater* 117, 2021. doi: 10.1016/j.diamond.2021.108458.



100. **Pari AA, Yousefi M.** Interactions between favipiravir and a BNC cage towards drug delivery applications. *Struct Chem* 33: 159–167, 2022. doi: 10.1007/s11224-021-01833-8.
101. **Piya AA, Ahmed T, Khaleque MdA, Ahmed K, Shamim SUD.** Trivalent and pentavalent atoms doped boron nitride nanosheets as Favipiravir drug carriers for the treatment of COVID-19 using computational approaches [Online]. *Comput Theor Chem* 1217: 113902–113902, 2022. <https://api.semanticscholar.org/CorpusID:252654306>.
102. **Zahid MN, Kosar N, Sajid H, Ibrahim KE, Gatasheh MK, Mahmood T.** Unveiling the Potential of B3O3 Nanoflake as Effective Transporter for the Antiviral Drug Favipiravir: Density Functional Theory Analysis. *Molecules* 28, 2023. doi: 10.3390/molecules28248092.
103. **Yao C, Xiang F, Xu Z.** Metal oxide nanocage as drug delivery systems for Favipiravir, as an effective drug for the treatment of COVID-19: a computational study. *J Mol Model* 28, 2022. doi: 10.1007/s00894-022-05054-6.
104. **Hasan MM, Das AC, Hossain MR, Hossain MK, Hossain MA, Neher B, Ahmed F.** The computational quantum mechanical investigation of the functionalized boron nitride nanocage as the smart carriers for favipiravir drug delivery: a DFT and QTAIM analysis. *J Biomol Struct Dyn* 40, 2022. doi: 10.1080/07391102.2021.1982776.



Data availability

Data from this study will be made available from the corresponding author upon reasonable request.

